

2024

Regime shifts in Arctic terrestrial hydrology manifested from impacts of climate warning

Michael A. Rawlins
University of Massachusetts Amherst

Ambarish V. Karmalkar
University of Massachusetts Amherst

Follow this and additional works at: https://scholarworks.umass.edu/geo_faculty_pubs

Recommended Citation

Rawlins, Michael A. and Karmalkar, Ambarish V., "Regime shifts in Arctic terrestrial hydrology manifested from impacts of climate warning" (2024). *The Cryosphere*. 38.
<https://doi.org/10.5194/tc-18-1033-2024>

This Article is brought to you for free and open access by the Geosciences at ScholarWorks@UMass Amherst. It has been accepted for inclusion in Geosciences Department Faculty Publication Series by an authorized administrator of ScholarWorks@UMass Amherst. For more information, please contact scholarworks@library.umass.edu.



Regime shifts in Arctic terrestrial hydrology manifested from impacts of climate warming

Michael A. Rawlins¹ and Ambarish V. Karmalkar^{2,1}

¹Department of Earth, Geographic, and Climate Sciences, University of Massachusetts, Amherst, MA 01003, USA

²Department of Geosciences, University of Rhode Island, Kingston, RI 02881, USA

Correspondence: Michael A. Rawlins (mrawlins@umass.edu)

Received: 5 June 2023 – Discussion started: 19 June 2023

Revised: 29 January 2024 – Accepted: 30 January 2024 – Published: 5 March 2024

Abstract. Anthropogenic warming in the Arctic is causing hydrological cycle intensification and permafrost thaw, with implications for flows of water, carbon, and energy from terrestrial biomes to coastal zones. To better understand the likely impacts of these changes, we used a hydrology model driven by meteorological data from atmospheric reanalysis and two global climate models for the period 1980–2100. The hydrology model accounts for soil freeze–thaw processes and was applied across the pan-Arctic drainage basin. The simulations point to greater changes over northernmost areas of the basin underlain by permafrost and to the western Arctic. An acceleration of simulated river discharge over the recent past is commensurate with trends drawn from observations and reported in other studies. Between early-century (2000–2019) and late-century (2080–2099) periods, the model simulations indicate an increase in annual total runoff of 17%–25%, while the proportion of runoff emanating from subsurface pathways is projected to increase by 13%–30%, with the largest changes noted in summer and autumn and across areas with permafrost. Most notably, runoff contributions to river discharge shift to northern parts of the Arctic Basin that contain greater amounts of soil carbon. Each season sees an increase in subsurface runoff; spring is the only season where surface runoff dominates the rise in total runoff, and summer experiences a decline in total runoff despite an increase in the subsurface component. The greater changes that are seen in areas where permafrost exists support the notion that increased soil thaw is shifting hydrological contributions to more subsurface flow. The manifestations of warming, hydrological cycle intensification, and permafrost thaw will impact Arctic terrestrial and coastal en-

vironments through altered river flows and the materials they transport.

1 Introduction

Hydrological cycle intensification and permafrost thaw are among a myriad of environmental changes reshaping the Arctic environment (Rawlins et al., 2010; Hinzman et al., 2013; Box et al., 2019; Overland et al., 2019). Climate forcings, including increasing air temperature and precipitation, are key drivers of alterations to the Arctic system (Box et al., 2019). The Arctic has warmed 2.5 to 4 times faster than the global average over the past several decades (Rantanen et al., 2022; Wang et al., 2022) and experienced substantial decreases in Arctic Ocean sea ice extent and volume (Stroeve and Notz, 2018; Serreze and Meier, 2019). Warming is leading to hydrologic intensification that is projected to drive higher precipitation rates (Bintanja and Selten, 2014; McCrystall et al., 2021), with concomitant rises in river discharge (Shiklomanov and Shiklomanov, 2003; Dankers and Middelkoop, 2008). Permafrost thaw has the potential to change how water is stored and moved and to mobilize vast stores of organic carbon sequestered in soils (Frey and Smith, 2005; Koch et al., 2022; Mohammed et al., 2022; Del Vecchio et al., 2024) and rising river discharge (Peterson et al., 2002; Wagner et al., 2011; Feng et al., 2021), furthermore implying associated changes in exports of water, energy, carbon, and other constituents to coastal zones (Tank et al., 2016; Behnke et al., 2021; Zhang et al., 2021). In light of these alterations, it is important to better understand how climate warming, hydrological cycle intensification, and per-

mafrost thaw will impact Arctic terrestrial hydrology and, in turn, exports of freshwater and associated materials through the Arctic drainage basin and into coastal zones.

The seasonal storage of precipitation in the form of snow is a defining element of Arctic hydrology, contributing to abundant surface water storages and high river flows following spring melt. The presence of permafrost is another important element influencing the region's water cycle. Climate warming is intensifying Earth's water cycle, increasing precipitation, evaporation, evapotranspiration (ET), and river discharge globally (Huntington, 2006, 2010) and across Arctic regions (Peterson et al., 2002; Déry et al., 2009; Rawlins et al., 2010). Intensification or "acceleration" involves the effects of both atmospheric moisture-holding capacity and moisture availability. Declining sea ice is making the Arctic Ocean and its surrounding seas a more available source of moisture, with locally driven precipitation recycling greatest in winter across the Beaufort, Chukchi, Laptev, Kara, and East Siberian seas (Ford and Frauenfeld, 2022). Increasing late summer precipitation and a shift toward rainfall runoff are occurring across watersheds in northwest Alaska (Arp et al., 2020; Rawlins, 2021; Arp and Whitman, 2022). Terrestrial hydrology in the Arctic is also strongly controlled by the presence of permafrost and the seasonal thawing and freezing of soils (Tananaev et al., 2020). Permafrost underlies approximately one-fifth of the global land area and influences processes involving runoff, aquatic biogeochemistry (Frey and McClelland, 2009; Spencer et al., 2015; Hu et al., 2023), and land-atmosphere greenhouse gas exchanges (Christensen et al., 2004; McKenzie et al., 2021). Permafrost acts as an impermeable hydrological barrier, helping to maintain high soil suprapermafrost moisture levels while reducing soil water storage capacity and constraining subsurface flow (Woo et al., 2008; Walvoord and Kurylyk, 2016). The presence or absence of permafrost and variability in precipitation processes leads to varying amounts of surface and subsurface runoff contributions to river discharge and, in turn, land-ocean exports of freshwater and associated materials. Warming is causing long-term changes in near-surface soil freeze-thaw cycles and permafrost (Anisimov and Reneva, 2006; Koven et al., 2013; Guo et al., 2018; Peng et al., 2018; Biskaborn et al., 2019), with implications for permafrost hydrology (Woo et al., 2008; Liljedahl et al., 2016; Lafrenière and Lamoureux, 2019; Jin et al., 2022). Subsidence due to thawing soils will likely lead to more runoff while also significantly accelerating drying of tundra landscapes in a warming climate (Painter et al., 2023). Studies suggest that permafrost degradation leads to increased moisture transport from the surface to deeper soils, potentially contributing to increased river baseflows (Walvoord and Striegl, 2007) and cold-season discharge (St. Jacques and Sauchyn, 2009; Shiklomanov et al., 2013; Tananaev et al., 2016; Rawlins et al., 2019; Debolskiy et al., 2021; Wang et al., 2021; Liu et al., 2022). In northwest Alaska, positive trends in air temperature and precipitation are greatest in autumn which, together with

permafrost thaw, are likely leading to enhanced subsurface suprapermafrost runoff during that time (Rawlins, 2021).

Climate models are essential tools for understanding how manifestations of climate warming will alter the Arctic's terrestrial hydrology and riverine land-ocean fluxes. Model projections point to future precipitation increases over the twenty-first century through enhanced regional evaporation, poleward moisture transport (Bintanja et al., 2020), and sea ice declines (Bintanja and Selten, 2014). Models with the strongest warming response point to decreased snowfall across the High (70–90°N) Arctic. The precipitation increases are firmly linked to Arctic warming and sea ice decline (Bintanja, 2018; Arp et al., 2020) and are likely to increase river discharge (Peterson et al., 2002; Zhang et al., 2013). Recent coordinated research programs have produced bias-corrected climate model data for historical and future conditions from consistent protocol frameworks (Warszawski et al., 2014; Lange, 2021). Simulations of permafrost dynamics and associated soil freeze-thaw processes require attention to several key processes absent in many land-surface models (Alexeev et al., 2007; Nicolsky et al., 2007; Lawrence and Slater, 2008). Slater and Lawrence (2013) concluded that, in general, permafrost is not well represented by the ensemble of CMIP5 models. Examining permafrost dynamics in global models participating in the CMIP6, Burke et al. (2020) found that simulations of active layer thickness (ALT) and other key features often fell outside the observed range, with errors attributable to shallow and poorly resolved soil profiles and structural weaknesses in snow physics and soil hydrology within some of the models.

In this study we use simulations with a permafrost hydrology model with sophisticated soil freeze-thaw algorithms that represent an improvement upon traditional land-surface models to evaluate how climate alterations linked to warming, primarily hydrological cycle intensification and permafrost thaw, will influence Arctic terrestrial hydrology and, in turn, land-ocean riverine freshwater and biogeochemical fluxes. We begin by examining meteorological data from climate models to understand the atmospheric forcings and their influence on surface hydrology. Model simulations are validated against select observations for sublimation, ET, ALT, and river discharge. We then examine changes over the twenty-first century to gain insights into how hydrological cycle intensification and permafrost thaw will impact key elements of Arctic terrestrial hydrology controlling river exports, and then we test the hypothesis that within the Arctic drainage basin, changes in subsurface runoff are greatest in permafrost areas.

2 Methods

2.1 Study area and spatial grid

The pan-Arctic drainage basin used in this study encompasses approximately 22.45×10^6 km². It has a wide range of land cover types, from grasslands in southern Canada and central Eurasia to boreal forests to tundra in far northern areas. This domain includes basins of rivers draining into the Arctic Ocean, Hudson Bay, and the Bering Strait, with the large Yukon River draining into the latter. The region's four largest rivers – the Ob, Yenisei, Lena, and Mackenzie – flow primarily in a south-to-north direction and account for roughly half (49%) of the pan-Arctic basin area. Model forcing data, simulations, and outputs were produced on the 25×25 km EASE-Grid (Equal Area Scalable Earth Grid; Brodzik and Knowles, 2002). The spatial domain encompassing the terrestrial pan-Arctic as defined in this study has 35 693 grid cells. Each grid cell has 23 vertical layers extending to a 60 m depth in which water and energy interact with the soil and vegetation. Thus, the model is set up and executed in three dimensions (2D horizontal and 1D vertical) like many similar land-surface models often used to quantify terrestrial hydrological fluxes.

2.2 Modeling approach

The modeling approach leverages simulations with the Permafrost Water Balance Model (PWBM v4) to investigate the impacts of warming, hydrological cycle intensification, and permafrost thaw on terrestrial hydrological fluxes within and through the pan-Arctic drainage basin. Many of the details of PWBM have been documented elsewhere, so a general description is provided here with the reader encouraged to obtain more detail from the cited literature. The PWBM simulates all major elements of the water cycle, including transpiration and soil and surface water evaporation, snow storage, sublimation (Rawlins et al., 2003, 2013), runoff (Rawlins et al., 2021), and soil freeze–thaw. Past applications include assessment of causes behind record Eurasian discharge (Rawlins et al., 2010), estimation of surface water dynamics (Schroeder et al., 2010), analysis of present and future water budgets (Clilverd et al., 2011), quantification of freshwater and dissolved organic carbon fluxes (Rawlins et al., 2021), investigation of trends in those fluxes to a coastal lagoon in northwest Alaska (Rawlins, 2021), and exploration of the links between surface organic soil properties and moisture dynamics across the Alaska North Slope (Yi et al., 2022). PWBM operates at an implicit daily time step, with meteorological forcings (air temperature, precipitation, and wind speed) typically drawn from reanalysis data for regional-scale simulations or, when applied to smaller watersheds, meteorological station data. Daily simulated ET depends on atmospheric demand and surface and soil conditions. In this study, we applied the Hamon method to estimate poten-

tial evapotranspiration. The model includes a surface water pool that is typically transient and most often occurs after snowmelt. Runoff is generated when (i) the amount of available water at the surface exceeds infiltration capacity, and (ii) the amount of water in a soil layer exceeds field capacity, which is a function of soil texture. The sum of surface and subsurface runoff from one or more soil layers within a grid cell constitutes daily total runoff. We use the term “subsurface runoff” for the water flux that has followed subsurface pathways into the stream. Subgrid fractions of inundated areas (lakes and ponds) are parameterized based on observed data (Du et al., 2016), with total runoff across each grid cell calculated as a weighted total from the inundated and non-inundated areas. We applied a simple river flow accumulation and linear routing model (Rawlins et al., 2019) to estimate the timing shift in discharge export at the coast. The snow model simulates the effects of seasonal changes in snow density and, in turn, snow thermal conductivity (Liston et al., 2007; Sturm et al., 1995). Soil freeze–thaw process representations include a multilayer soil module with algorithms for unfrozen water dynamics and phase change, as well as specification of the thermal and hydrological properties of organic soils (Sazonova and Romanovsky, 2003; Nicolsky et al., 2007). The PWBM has a 60 m soil column, includes parameterizations for thermal and hydraulic properties of organic soils, and simulates the effect of depth hoar and wind compaction on snow density. Rawlins et al. (2013) describe the soil freeze–thaw and snow algorithms and calibration procedures, which involve factors controlling ET, snow sublimation, and subsurface runoff that differ between forest and tundra landscapes. In this study each transient simulation was preceded by a 50-year spin-up in year 1980 to stabilize soil temperature, moisture, and soil dissolved organic carbon (DOC) pools. While parameterizations for fields such as soil texture and vegetation cover are fundamental elements of land-surface and hydrological model simulations, simulated runoff in Arctic regions is most sensitive to the time-varying meteorological forcings (Rawlins et al., 2003).

Permafrost extent is based on end-of-season soil temperatures. If the soil column down to the maximum 60 m depth is frozen, beneath a thawed upper zone (i.e., active layer), the grid cell is deemed to have permafrost that year. Thus, permafrost state is a binary classification. In the case where soil temperatures are well simulated, one can assume that there is discontinuous permafrost in regions where many grid cells classified as permafrost interface with many grid cells classified as seasonally frozen. The impact of subsidence on permafrost thaw is not accounted for in the simulations, though the effect may be relatively small (Painter et al., 2023), particularly in areas lacking polygonal tundra. In models operating at continental scales, estimates of permafrost extent across transition zones between continuous permafrost and the non-permafrost areas are more uncertain due to limitations resolving spatial variations.

2.3 Meteorological forcings

This study focuses on numerical model simulations that were forced with gridded meteorological data (Table 1). We begin by examining simulations forced with reanalysis data to characterize dynamics over the recent past. Changes over the twenty-first century were assessed using the PWBM simulations forced with meteorological data from the coupled climate models, rather than the hydrology outputs (e.g., runoff) from the models, as outputs from individual models can vary widely and often imply unrealistic long-term systematic changes in water storage and water level within entire basins (Bring et al., 2015).

Simulations were made using forcings from three reanalysis datasets (W5E5, ERA5, MERRA) and two global climate models from the Coupled Model Intercomparison Project Phase 6 (CMIP6). The WFDE5 data – WATCH Forcing Data methodology applied to ERA5 reanalysis – are bias-adjusted ERA5 data at $0.5^\circ \times 0.5^\circ$ spatial and subdaily resolutions, generated specifically to be used as climate data inputs for impacts studies (Cucchi et al., 2020). The WFDE5 data over land are merged with ERA5 data over the ocean to produce W5E5 data (Lange, 2019a), compiled as part of phase 3b of the Inter-Sectoral Impact Model Intercomparison Project (ISIMIP3b) (Lange, 2019a, 2021). We downloaded and analyzed the W5E5 version 2 data for use as meteorological forcings for simulations over the historical period. We use bias-adjusted data (W5E5 v2 and climate models) prepared as part of the ISIMIP framework (Cucchi et al., 2020; Lange et al., 2021). We also applied data from the ERA5 and MERRA reanalysis to gauge the accuracy of the air temperature (2 m), precipitation, and wind speed forcings and for model validation. Precipitation amounts in the W5E5 data are lowest among the three reanalysis datasets. To ameliorate this bias in the simulation forced with W5E5, we increased each precipitation value by 20%. The ISIMIP3b climate model forcing data are bias adjusted and statistically down-scaled, and they are available for five CMIP6 models (GFDL-ESM4, IPSL-CM6A-LR, MPI-ESM1-2-HR, MRI-ESM2-0, UKESM1-0-LL) forced with three Shared Socioeconomic Pathways (SSP) scenarios (SSP1-2.6, SSP3-7.0, SSP5-8.5). In our two simulations over the years 1980–2100, we used data from two models (MPI-ESM1-2-HR, IPSL-CM6A-LR) forced with SSP3-7.0, which is a high-emissions business-as-usual scenario that is suitable in investigating the response of Arctic hydrology to a strong climate forcing. These two climate models generally bracket the range of climate projections for the pan-Arctic region across the five CMIP6 models (Fig. S1). The selection of these two models – hereafter IPSL and MPI – is aimed at capturing a wide range of temperature and precipitation projections but not necessarily the full range. Air temperature and precipitation changes expressed by the models are described in Sect. 4.1 and 4.2, respectively. In a study examining which CMIP3 models performed best at capturing meteorological quantities across parts of the Arc-

tic, a predecessor of the MPI-ESM ranked highest (Walsh et al., 2008).

2.4 Statistical analysis

Our analysis of changes closely connected to Arctic rivers centers on differences between 20-year intervals representing conditions for early (2000–2019) and late (2080–2099) periods in the century. Specifically, we mapped climatological averages over these periods and examined the differences for each domain grid cell. Domain-wide averages were computed from all 35 693 grid cells covering the domain. The statistical significance of differences between the two periods was calculated for select quantities. Before applying the statistical significance test, we used graphical analysis and the Shapiro–Wilk test (Shapiro and Wilk, 1965) to determine if the data series of interest is approximately normally distributed. The paired t test was then applied to test the null hypothesis that the mean difference between two variables is 0. The relative (percentage) difference is calculated based on the following standard formula: relative difference (%) = $(Z_2 - Z_1) / Z_1 \times 100$, where Z_1 and Z_2 are values for early and late periods, respectively.

Metrics which rely on squared differences are known to be problematic (Willmott and Matsuura, 2005; Hodson, 2022). The RMSE in particular is inappropriate because it is a function of three characteristics of a set of errors, rather than of one error (the average error). The RMSE varies with the variability within the distribution of error magnitudes and with the square root of the number of errors, as well as with the mean absolute error (MAE) magnitude. Interpretation problems can thus arise because sums-of-squares-based statistics do not satisfy the triangle inequality (Willmott and Matsuura, 2009). Thus MAE and mean bias error (MBE) are more natural measures of average error, and evaluations and intercomparisons in this study are based upon it.

In this study, we leverage the simulations forced by the two climate models to investigate the sensitivity of thermal and hydrological responses to different climate forcings. We do not do this to provide robust quantitative projections, which would require a multimodel, multi-scenario ensemble.

3 Model validation

We first compared key components of the simulated water budget – active layer thickness, sublimation, evapotranspiration, and discharge – with different observational datasets to assess the credibility of the PWBM simulations. Simulated active layer thickness (ALT) and model-estimated permafrost extent are compared to ALT data from the National Tibetan Plateau / Third Pole Environment Data Center (TPDC) (Fig. 1a–d) and permafrost area from the International Permafrost Association (IPA) data. In this study, the active layer is the top layer of ground subject to annual thawing and freez-

Table 1. Simulations conducted in the study time period for the transient simulation and origin of forcing data. Each transient simulation was preceded by a 50-year spin-up. For the climate model forcing, the 1980–2100 period includes two different experiments.

Model simulations		
Name	Period	Forcing
PWBM-W5E5	1980–2019	Bias-adjusted ECMWF Reanalysis v5 (ERA5)
PWBM-ERA5	1980–2019	ERA5 Reanalysis
PWBM-MERRA	1980–2013	Modern-Era Retrospective Analysis for Research and Applications
PWBM-IPSL	1980–2100	IPSL-CM6A-LR (Historical: 1980–2014; SSP3-7.0: 2015–2100)
PWBM-MPI	1980–2100	MPI-ESM1-2-HR (Historical: 1980–2014; SSP3-7.0: 2015–2100)

ing in areas underlain by permafrost. Simulated ALT in the model simulations spans a greater range compared with the TPDC data (Fig. 1e). However, the TPDC ALT estimates are known to have a reduced distribution range, owing to the machine learning approach used (Ni et al., 2021). As Ran et al. (2022) described in their analysis of the TPDC dataset, the uncertainty of ALT is considerable, especially in the vast area of western Siberia where the training data are sparse. Further, they suggested that the low spatial representativeness of training data may have led to an overestimation in several Siberian mountain regions and an underestimation near the lower boundary of permafrost. Moreover, in situ ALT is obtained at a point location that may not be representative of the region in which it is located. In light of these uncertainties, permafrost extent is generally well captured, with differences from the total area of continuous and discontinuous permafrost in the IPA dataset of less than 10 % (Table 2). For comparison, the fraction of continuous, discontinuous, and sporadic or isolated permafrost within the major river basins is shown in Table 3. In Eurasia, there exists a clear west–east gradient, with the relatively cold Lena River basin having a large amount of continuous permafrost. In North America, the Mackenzie River basin has a large extent of land in the south devoid of permafrost, which is a reflection of the relatively warm climate there.

We used the simulation forced with W5E5 data (PWBM-W5E5) to evaluate the magnitude of vertical fluxes of water from sublimation and ET over the recent past (Fig. 2). Overestimates in simulated sublimation (Fig. S2a) are noted (domain-wide average sublimation of 40 mm yr^{-1} for GLEAM (Global Land Evaporation Amsterdam Model) and 57 mm yr^{-1} for PWBM-W5E5), though the discrepancy is small relative to the magnitudes of annual total runoff and ET ($\text{MAE} = 27 \text{ mm yr}^{-1}$). Simulated ET (260 mm yr^{-1}) generally falls between the estimates from GLEAM (304 mm yr^{-1}) and remote-sensing-based data (230 mm yr^{-1}), which include differences of 14 % and 12 % (MAE of 64 and 198 mm yr^{-1}), respectively. The model generally captures the spatial pattern in sublimation and ET, though regionally there are notable differences, particularly across the warmer southerly areas where PWBM tends to underestimate ET (Fig. S2b, c). For runoff, this result points to

Table 2. Permafrost areal extent and difference from observed extent across the study domain. Area (in 10^6 km^2) from the International Permafrost Association (IPA) classification (Brown et al., 2001), the National Tibetan Plateau / Third Pole Environment Data Center (TPDC) dataset (Ran et al., 2022), and PWBM simulations. Areas of continuous and discontinuous permafrost were added for the IPA estimate. Difference is defined based on observations from the IPA-based extent. For the simulated estimates, a grid cell is deemed to have permafrost under the standard definition of ground (model soil layer) that remains at or below 0°C for at least 2 consecutive years.

Data	Area (10^6 km^2)	Difference (%)
IPA	13.2	–
TPDC	12.5	–5.5
PWBM-W5E5	12.7	–4.2
PWBM-ERA5	13.1	–0.8
PWBM-MERRA	10.5	–20.4
PWBM-IPSL	12.4	–6.2
PWBM-MPI	11.8	–10.9

Table 3. Permafrost coverage by class in percent (%) for major river basins of the terrestrial pan-Arctic. The fraction of land without permafrost is in column non-PF.

Basin	Continuous	Discontinuous	Sporadic/ isolated	Non-PF
Ob	4.3	3.8	5.0	86.9
Yenisei	31.9	11.0	51.9	5.2
Lena	77.4	12.9	9.4	0.3
Mackenzie	15.7	29.6	47.3	7.4
Yukon	18.8	68.1	13.1	0.0

a possible wet bias in those areas relative to observed conditions.

We compared simulated discharge volume to a new dataset, the Remotely sensed Arctic Discharge Reanalysis (RADR), that was generated through assimilation of approximately 9.18 million discharge observations derived from 227 million river width measurements from Landsat images (Feng et al., 2021). Simulated discharge volume is the sum total of runoff over the contributing river basin. This evalu-

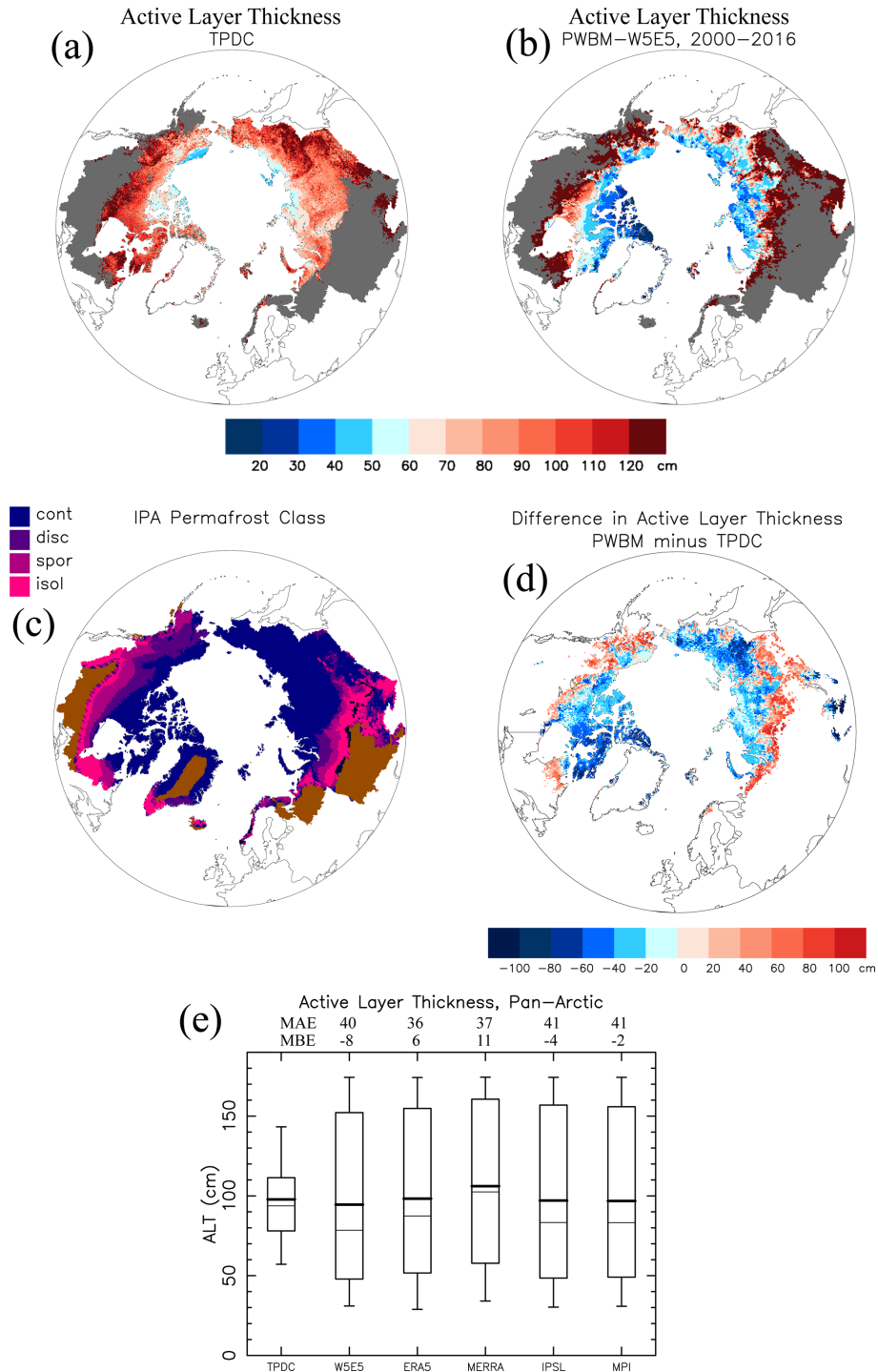


Figure 1. (a) Active layer thickness (ALT; cm) from the TPDC database (Ran et al., 2022) for the period 2000–2016 and (b) from the PWBM simulation forced with W5E5 data over same period. Grey shading indicates non-permafrost areas. (c) Permafrost classification from International Permafrost Association (IPA) data. (d) Difference in ALT (cm) between PWBM and TPDC. (e) Distributions of annual maximum ALT (cm) for all grids with permafrost. ALT is the average for each year over the period 2000–2016. TPDC is used as validation for the ALT estimated by simulations forced with data from W5E5, ERA5, MERRA (2000–2013), IPSL, and MPI. Box plot rectangles bracket the 25th and 75th percentiles. Whiskers extend to the 5th and 95th percentiles. Thick and thin horizontal lines mark the distribution mean and median, respectively. The mean absolute error (MAE; cm) and mean bias error are (MBE; cm) shown.

ation was performed for total discharge from the pan-Arctic drainage basin and five large Arctic rivers: the Ob, Yenisei, Lena, Mackenzie, and Yukon (Fig. S3). The model tends to overestimate discharge across western Eurasia and underestimate it across eastern Eurasia. Differences are modest for the two North American rivers. However, the magnitude of pan-Arctic discharge is well constrained. Average freshwater export to the Arctic Ocean from the study domain over the period 1984–2018 is $5169 \text{ km}^3 \text{ yr}^{-1}$ based on RADR. Over the same period, annual total discharge is 5752, 5822, and $5811 \text{ km}^3 \text{ yr}^{-1}$ in the simulations forced by W5E5, IPSL, and MPI, respectively (Fig. S4), giving differences from RADR discharge of less than 13%. The simulation forced with W5E5 captures the acceleration in Arctic discharge reported in other studies (Peterson et al., 2002; Feng et al., 2021). The linear trend of $8.3 \text{ km}^3 \text{ yr}^{-2}$ ($0.15 \% \text{ yr}^{-1}$) closely aligns with the acceleration ($11.6 \text{ km}^3 \text{ yr}^{-2}$, $0.22 \% \text{ yr}^{-1}$) from RADR discharge (Feng et al., 2021), and it is in the upper range of estimates ($3.5\text{--}10 \text{ km}^3 \text{ yr}^{-2}$) from prior studies (Shiklomanov et al., 2000; McClelland et al., 2006; Rawlins et al., 2010).

For comparison, an analysis of the four largest Arctic-draining rivers (Mackenzie, Ob, Yenisei, and Lena) indicates that the combined annual discharge increased by 89 km^3 per decade over the period 1980–2009, amounting to an approximate 14% increase over the 30-year period (Ahmed et al., 2020). Hydrological cycle intensification is connected with warming and also manifested by increases in vertical fluxes of precipitation and ET. The differences of less than 15% between model-simulated ET and discharge, and the estimates from the validation datasets, suggest that the water budget components are sufficiently well constrained to enable evaluation of the impact of climate warming on runoff and river discharge in Arctic rivers. In general, the comparisons with observations support the model's ability to reliably simulate key hydrological variables of interest.

4 Alterations connected to hydrological cycle intensification and permafrost thaw

4.1 Air temperature

In this analysis, we use the simulations forced by the two climate models to bracket changes likely to occur this century, focusing primarily on 20-year periods representing conditions for early (2000–2019) and late (2080–2099) periods in the century. The IPSL model projects stronger warming compared to MPI, with warming measurements of $7.2 \text{ }^\circ\text{C}$ (domain-wide mean value) and $6.2 \text{ }^\circ\text{C}$ occurring between the early and late century, respectively. (Table 4). Both show the strongest warming over the highest latitudes of the pan-Arctic basin, with warming of over $10 \text{ }^\circ\text{C}$ across far northern Canada projected by IPSL. More modest warming of $3\text{--}4 \text{ }^\circ\text{C}$

is noted over southwestern Canada and central Eurasia in the MPI data.

In the results that follow, unless otherwise noted, statements reporting two statistics will be written in order for PWBM-MPI and PWBM-IPSL. In nearly every instance, changes are greater with the latter simulation due to the influence of forcing from the more strongly warming (and wetter) IPSL climate model.

4.2 Precipitation

Rainfall rates have also been increasing across much of the pan-Arctic. Rainfall will continue to increase this century, particularly along favored storm track regions over northwestern Eurasia and western Alaska (Fig. 3a, S5a) where the majority of water vapor transport into the Arctic occurs (Nash et al., 2018). Climatological average rainfall (domain average) is higher by the late century, with relative differences of 17% and 31% for the MPI and IPSL models, respectively (Table 4).

Snowfall is projected to increase over a smaller geographic extent, mainly in the higher latitudes and across the colder parts of eastern Eurasia, and decrease over most of the pan-Arctic, most prominently in western Eurasia and southern Canada (Figs. 3b, S5b). The domain-wide change averages 5% and 7%. The sizable rainfall increases drive the projected rise in the fraction of rainfall to total precipitation (Figs. 3c, S5c), averaging 11% and 47% for the two simulations. Net precipitation – the difference between precipitation and the sum of evapotranspiration and snow sublimation – is projected to increase across most ($> 75\%$) of the pan-Arctic basin. Decreases will occur across southern Canada and Eurasia. For areas with and without permafrost, mean changes (increases) are 31% and 42%, and 5% and 6%, respectively. The simulations thus reveal bigger impacts – a net wetting – over permafrost regions and a strong latitudinal south–north gradient in future precipitation changes that will influence river discharge quantity and quality.

4.3 Permafrost extent and active layer thickness

Research studies have documented hydrological cycle intensification and permafrost thaw across the terrestrial Arctic. To better understand changes in permafrost hydrology attributable to warming and increasing soil thaw, we calculated ALT averages from the two climate-model-forced simulations (Figs. 4, S6). For PWBM-IPSL, the permafrost area decreases by $7.8 \times 10^6 \text{ km}^2$ (12.3 to $4.5 \times 10^6 \text{ km}^2$) from the early- to late-century periods, a decline of 63% of present-day permafrost area. For PWBM-MPI, some $4.9 \times 10^6 \text{ km}^2$, or 42% of present area, loses permafrost (11.7 to $6.8 \times 10^6 \text{ km}^2$). Predictions of soil temperature from CMIP5 models point to permafrost fractional losses by the end of the century of 15% to 87% for RCP4.5 and 30% to 99% for RCP8.5 (Koven et al., 2013). Across areas that maintain per-

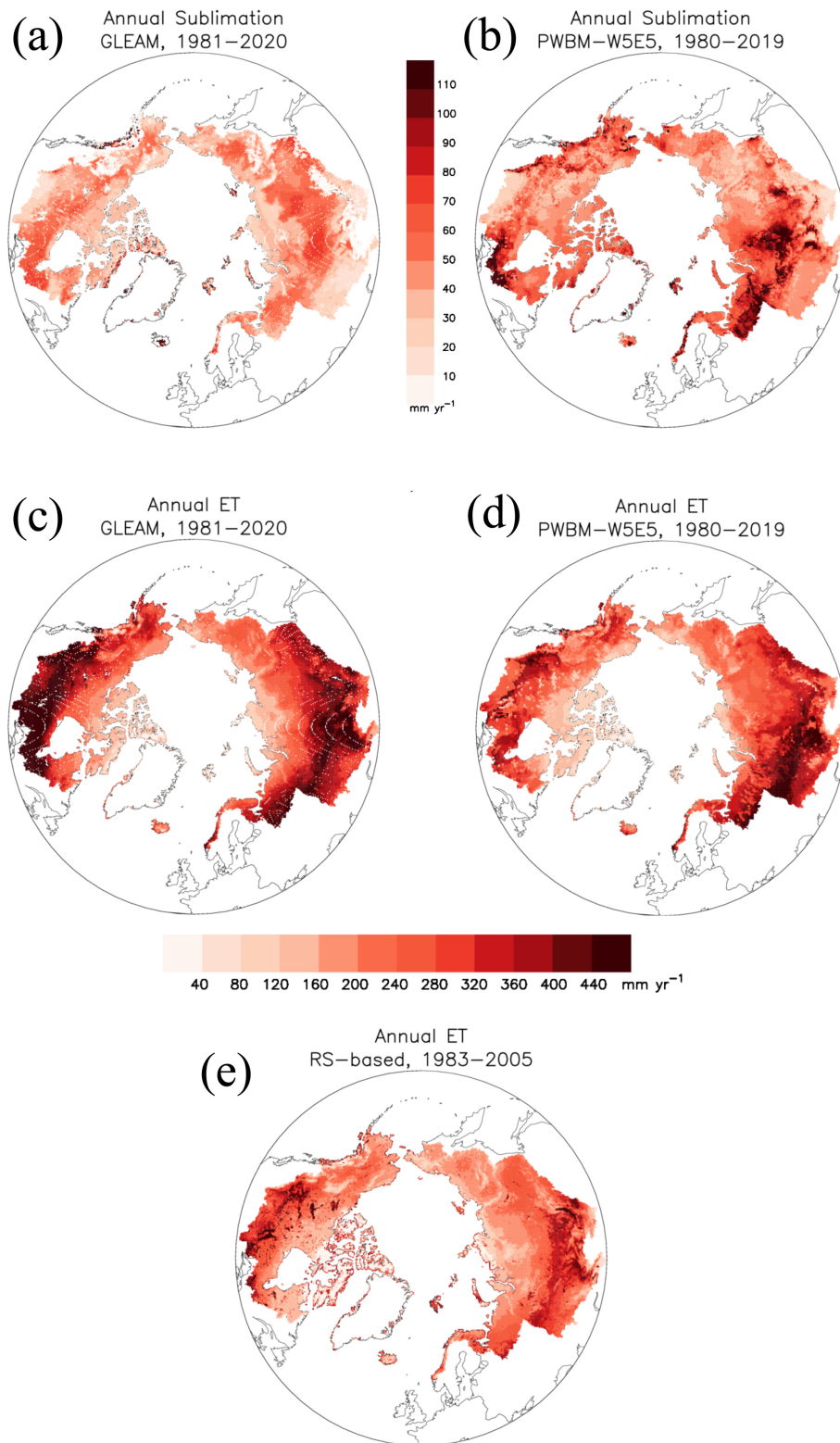


Figure 2. (a) Annual total sublimation (mm yr^{-1}) and (c) evapotranspiration (ET, mm yr^{-1}) from GLEAM (Miralles et al., 2011; Martens et al., 2017) and PWBM-W5E5 (b, d). Panel (e) shows ET from a dataset derived from remote-sensing data (Zhang et al., 2009).

Table 4. Climatological averages representing conditions for early (2000–2019) and late (2080–2099) periods in the century from the simulations forced with IPSL and MPI meteorological data.

Variable	PWBM-IPSL			PWBM-MPI		
	Early	Late	% diff*	Early	Late	% diff*
Air temp (C)	-5.3	1.9	7.2	-5.3	-0.9	6.2
Precipitation (mm yr ⁻¹)	578	697	21	573	643	12
Net precipitation (mm yr ⁻¹)	258	315	22	259	300	16
Rainfall (mm yr ⁻¹)	334	437	31	354	413	17
Snowfall (mm yr ⁻¹)	244	260	7	219	230	5
Rainfall fraction (%)	56	62	11	43	63	47
Runoff (mm yr ⁻¹)	264	329	25	266	310	17
<i>F</i> _{sub} (%)	27	35	30	30	34	13

* Relative (percentage) difference shown for each except air temperature, which is shown in degrees Celsius. Differences are statistically significant for all quantities listed based on the paired *t* test (Sect. 2.4).

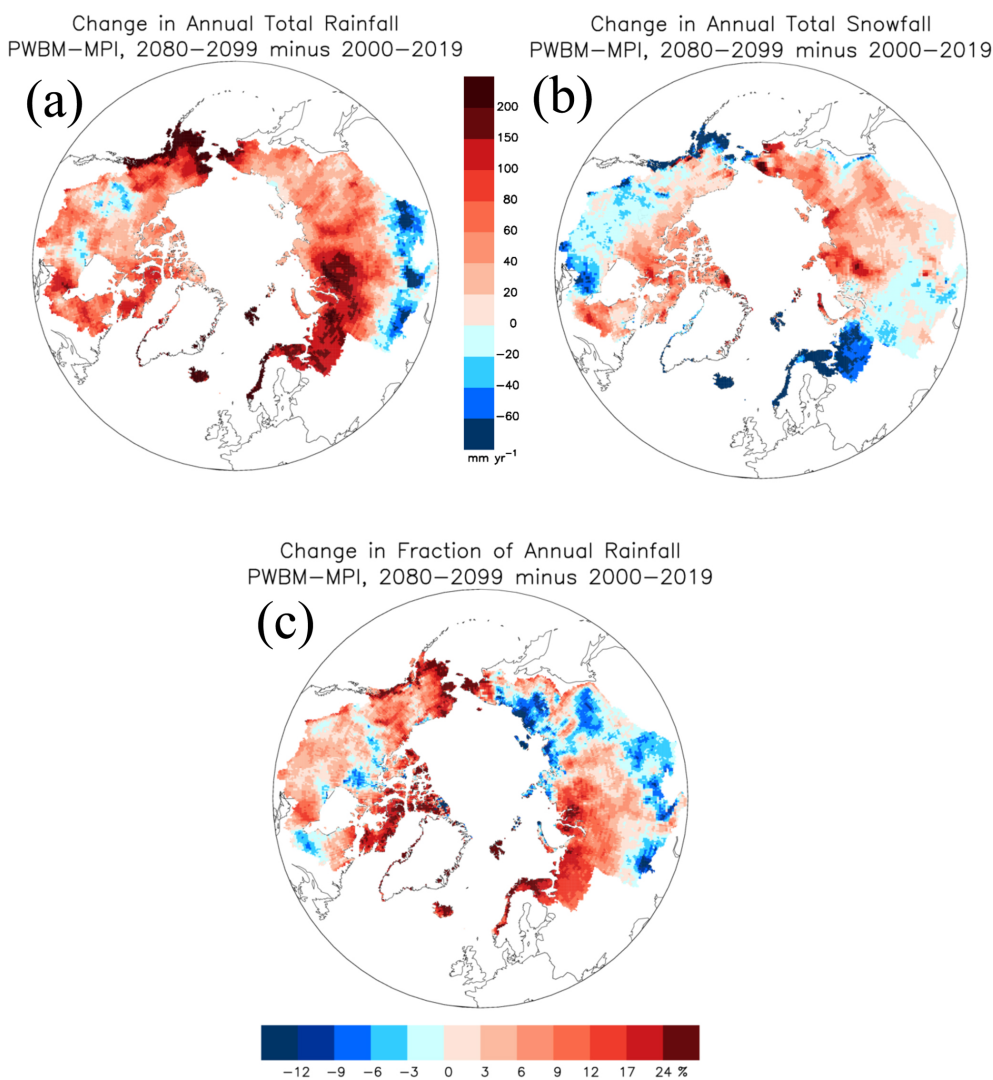


Figure 3. Change in (a) annual rainfall (mm yr⁻¹), (b) annual snowfall (mm yr⁻¹), and (c) the fraction of rainfall to total precipitation from the PWBM-MPI simulation.

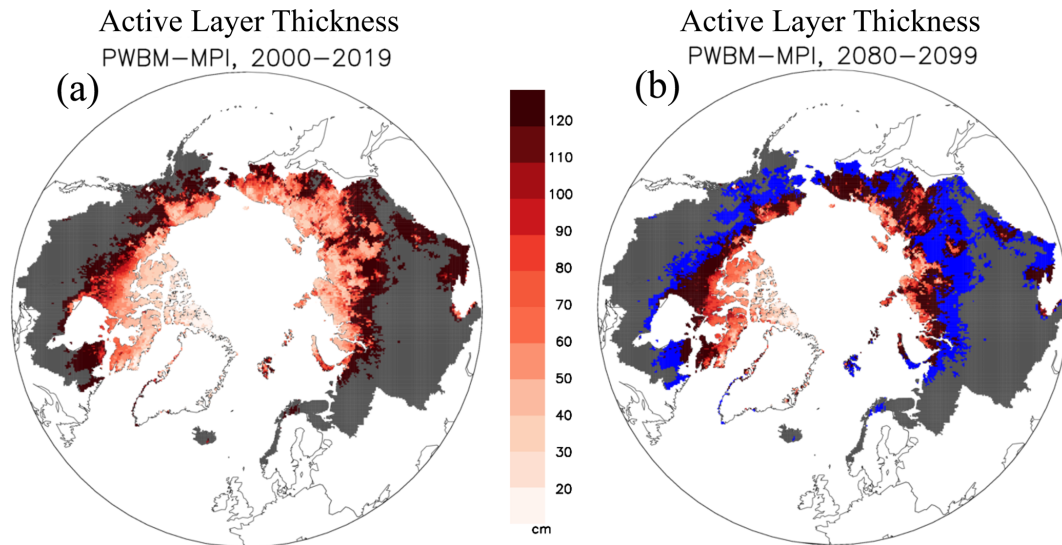


Figure 4. Simulated active layer thickness (ALT; cm) representing conditions for (a) early (2000–2019) and (b) late (2080–2099) periods in the century from PWBM-MPI. Blue shading highlights areas that are no longer characterized as permafrost in the future period. Grey areas are non-permafrost areas of the Arctic Basin.

mafrost, the ALT increases between the two periods average 56 and 91 cm. For comparison, estimates over permafrost areas obtained from an air-temperature-based thawing index applied to 16 CMIP5 models (2006–2100) forced under RCP8.5 averaged a similar 6.5 cm per decade.

4.4 Runoff and river discharge

Annual runoff within the pan-Arctic basin is typically highest across eastern Canada, western Eurasia, and coastal regions of western Canada and western Alaska. Runoff changes between the early- and late-century periods were calculated here to assess future alterations to river discharge (Figs. 5a, S7a). In Eurasia the change in annual total runoff, as a percent of the early period, is greater over northeast parts of the continent. Across North America the increases are also greater in the colder northern parts of the Canadian Archipelago and over northern Alaska. Averaged across all grid cells, annual runoff increases by 19 % (45 mm yr⁻¹) and 31 % (65 mm yr⁻¹) from PWBM-MPI and PWBM-IPSL, respectively. Not surprisingly, the spatial pattern in runoff change closely aligns with the pattern in net precipitation.

There is also a significant difference in the mean change in annual runoff between grid cells with permafrost (67 and 99 mm yr⁻¹ increase) and those without permafrost (21 and 25 mm yr⁻¹). This divergence is driven by changes in net precipitation (64 and 89 mm yr⁻¹ vs. 18 and 19 mm yr⁻¹), as well as differing influences from deepening ALT and longer thawed periods in areas with and without permafrost. Across permafrost areas, the difference between net precipitation and runoff – in a water budget, an approximation for change in storage – is 3–10 mm yr⁻¹, a small amount rel-

ative to the runoff increase. Over the early century period, river discharge volume is 5839, 5955, and 5917 km³ yr⁻¹ for the PWBM-W5E5, PWBM-MPI, and PWBM-IPSL simulations, respectively (Fig. S4). By the late century, discharge volume increases to 6955 and 7374 km³ yr⁻¹, which are relative increases of 17 % and 25 % for the PWBM-MPI and PWBM-IPSL simulations, respectively (runoff equivalents in Table 4). The trend is statistically significant ($p < 0.01$) for both time series.

A transition from runoff dominated by surface water contributions toward increasing amounts of subsurface flow is expected as the climate warms (Frey and McClelland, 2009). Compared to change in total runoff, the change in the fraction of subsurface to total runoff (F_{sub}) is more spatially variable across the pan-Arctic (Figs. 5b, S7b). During the early-century period, F_{sub} averages 30 % and 27 % in the PWBM-MPI and PWBM-IPSL simulations, respectively (Fig. 6). The fractions increase to 34 % and 35 % by the end of the century, giving a relative (percent) increase in domain mean F_{sub} of 13 % and 30 % for PWBM-MPI and PWBM-IPSL, respectively.

Based on the modest warming PWBM-MPI run, approximately 72 % of permafrost areas will have higher subsurface runoff fractions by the end of the century. This spatial extent increases to 88 % of the permafrost region under the more aggressive warming depicted under PWBM-IPSL (Fig. S7b). The shift in F_{sub} is larger in permafrost areas, with significant differences in spatial mean F_{sub} in areas with and without permafrost (relative differences of 15.7 % and 13.5 % for PWBM-MPI and 31.1 % and 24.4 % for PWBM-IPSL). The PWBM-MPI simulation reveals a significant relationship ($p < 0.01$) between change in ALT and F_{sub} , with

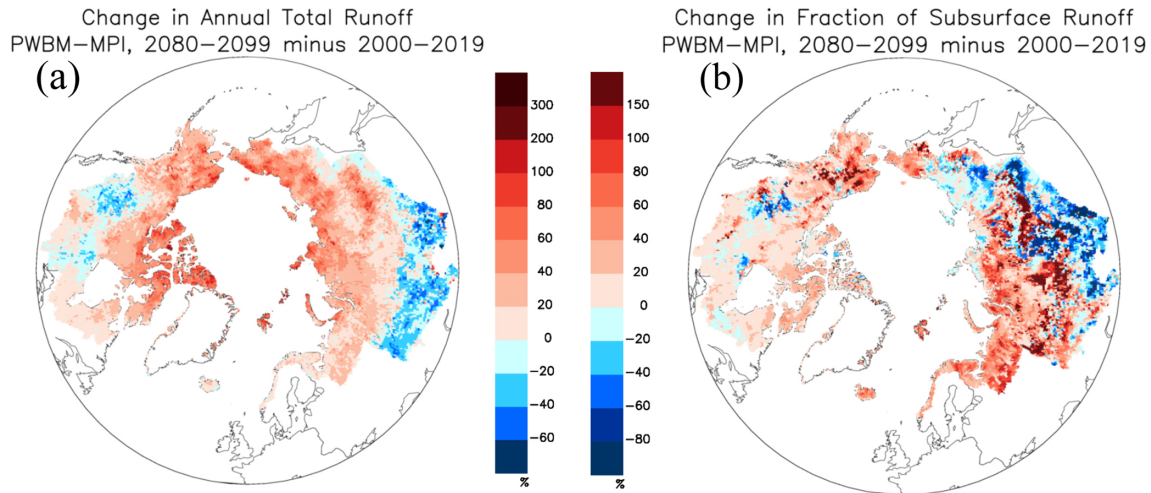


Figure 5. Change in (a) annual total runoff (%) and (b) fraction of subsurface to total runoff (F_{sub} ; %) from the simulations.

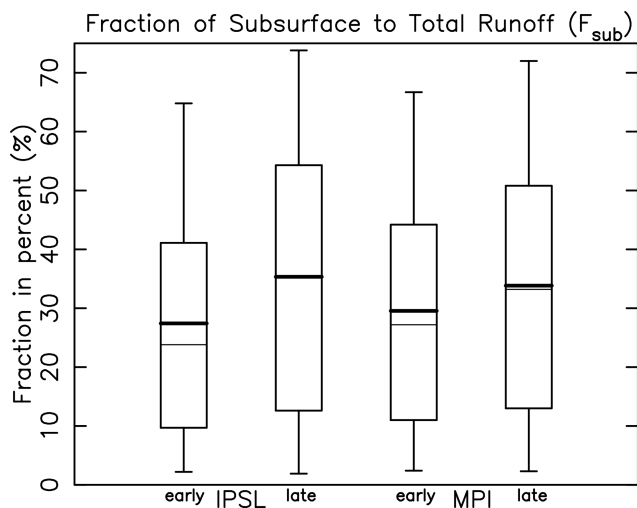


Figure 6. Fraction of subsurface to total runoff (F_{sub}) for early- and late-century periods for all pan-Arctic grids from PWBM-IPSL and PWBM-MPI simulations.

a 6.4% increase in F_{sub} per 0.1 m increase in ALT. While the positive correlation does not exist under PWBM-IPSL, the more pervasive growth in F_{sub} in PWBM-MPI suggests a connection between soil thaw and increasing contributions from subsurface runoff to river discharge during this century, particularly in regions underlain by permafrost.

The runoff changes in both simulations exhibit a significant positive relationship with latitude (Figs. 7a, S8a). The linear fit suggests an additional 2.9% and 4.2% runoff (PWBM-MPI and PWBM-IPSL) for each degree northward in latitude. Under this pattern, river discharge shifts over time to being sourced more from the northerly parts of the four largest river basins (Ob, Yenisei, Lena, and Mackenzie; Figs. 8a, S9a, and Table 5).

Decreases are projected for the southerly half of the Ob, Yenisei, and Mackenzie rivers. For the Ob River basin, less runoff across the southern half of the river basin will be offset by a higher flow in the north so that annual total discharge exported at the coast is relatively unchanged. The Yenisei shows a similar pattern, with accumulated discharge at the coast higher by the late century. The Lena and Mackenzie rivers will receive substantial additional discharge from their northern areas, with the Lena River basin projected to export 66 and 128 km³ yr⁻¹ (16% and 31%) more freshwater discharge by the late century. The sharp increase in export from the Yenisei and Lena river basins arising from their northern watersheds is driven primarily by higher snowfall rates (Figs. 3b, S5b). Averaged across the four, the downstream half of the rivers will receive approximately 20%–30% more accumulated discharge from the northern half of their contributing area. A south–north gradient also exists in soil carbon storage in these basins, with the highest amounts in the far north (Figs. 8b, S9b). Subsurface runoff increases are also greater to the north (Figs. 7b, S8b), though the scatter is substantial compared to the change in annual total runoff.

Runoff is projected to increase during most months in both simulations (Figs. 9, S10), with monthly changes remarkably similar between the two runs. Averaged over seasons, runoff increases (depth in mm) are greatest in spring (MAM). The increase in spring, particularly during May, is attributable to the additional snowmelt runoff and a shift to earlier snowpack melting. As a consequence, less snowmelt and runoff occur in June. Averaged across the six largest rivers (Ob, Yenisei, Lena, Mackenzie, Yukon, and Kolyma), peak daily discharge at each coastal outlet shifts earlier by the end of the century by approximately 11 d in both simulations (DOY 180 to 169 in PWBM-IPSL and DOY 176 to 165 in PWBM-MPI). Runoff is largely unchanged in July, August, and September, and the changes are not statistically signifi-

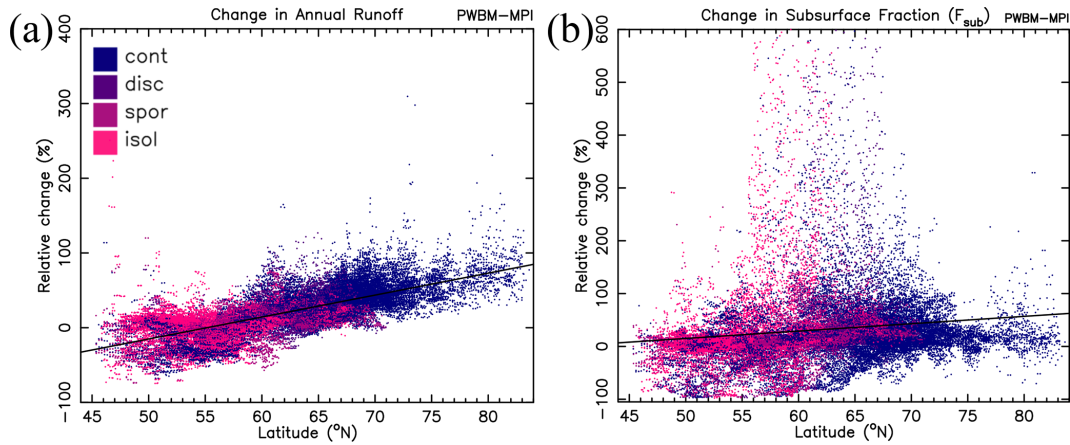


Figure 7. Change in (a) annual total runoff (%) and (b) F_{sub} , with grid cell latitude from the PWBM-MPI simulation for all pan-Arctic domain grid cells. Colors indicate permafrost classification (continuous, discontinuous, sporadic, or isolated) for the cell from the IPA dataset (Fig. 1c).

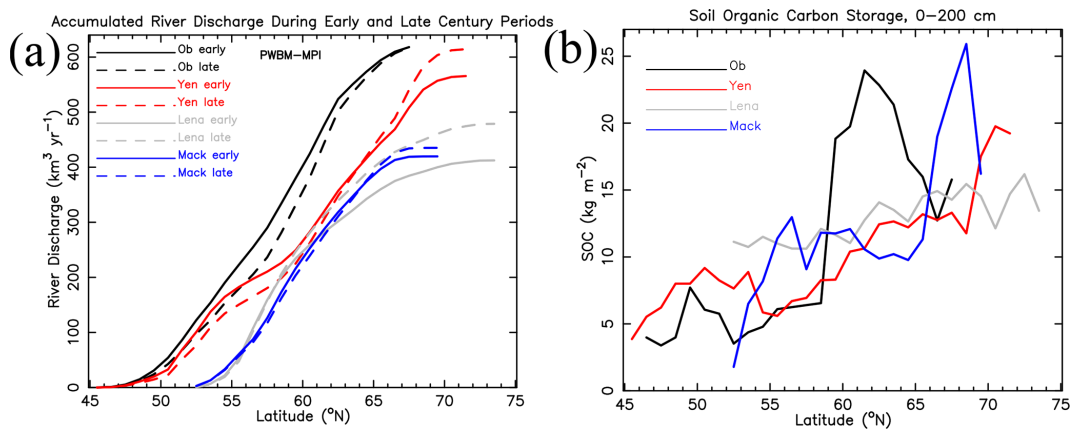


Figure 8. (a) Accumulated annual total river discharge ($\text{km}^3 \text{yr}^{-1}$) for the Ob, Yenisei, Lena, and Mackenzie rivers for 1° latitude bands as averages over early-century (solid line) and late-century (dashed) periods from PWBM-MPI. (b) Soil carbon storage (kg m^{-2}) in soil zones that are at 0–200 cm depth from the Northern Circumpolar Soil Carbon Database (Hugelius et al., 2013).

Table 5. Relative (percentage) change in accumulated river discharge for the upstream (southern) half and downstream (northern) half of each of the four largest Arctic rivers. Averages are calculated from the totals shown in Figs. 8, S7. The total row represents the average of the four.

River	PWBM-IPSL		PWBM-MPI	
	Up (%)	Down (%)	Up (%)	Down (%)
Ob	-9.8	7.4	-19.4	13.6
Yenisei	-1.5	27.9	-14.2	22.2
Lena	26.4	43.8	12.5	25.9
Mackenzie	-0.2	35.3	-5.3	17.3
Total	3.7	28.6	-6.6	19.7

cant in June and July due to the high degree of spatial variability. Seasonally, the relative change (percentage change) is greatest in winter, with runoff by the late-century period averaging a factor of 5–10 greater compared to the early-century period averages. Significant percentage increases are noted in autumn and spring as well. Interestingly, snow storage (snow water equivalent, SWE) increases in both simulations are significant in February, March, and April only. Notably, no increase in SWE is projected during autumn.

The intensifying hydrological cycle and thawing permafrost will manifest in changing amounts of surface and subsurface runoff contributions to river discharge (Fig. 10). The shifts vary strongly with season, and spatially across the terrestrial Arctic, with remarkably similar change in magnitudes in the two simulations due largely to similarities in patterns in net precipitation and its change this century. At the pan-Arctic scale, modest increases are projected in both sur-

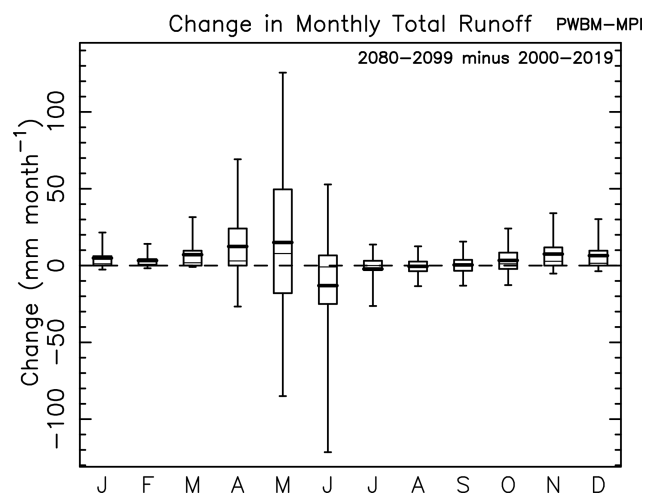


Figure 9. Distribution in change in monthly total runoff (mm month^{-1}) between early- and late-century periods for all pan-Arctic grid cells from PWBM-MPI.

face and subsurface runoff for the annual total and in winter, spring, and autumn. The acceleration during winter and autumn will come predominantly from additional subsurface runoff. Spring increases are mainly attributable to increased surface runoff. Runoff is projected to decrease slightly in summer due to less surface runoff, despite a small increase in subsurface runoff. The autumn change is particularly noteworthy over northern Alaska: there, summer shows a strong shift from surface to subsurface runoff. Runoff decreases are projected to occur in most seasons over southwest Canada, owing to relatively large precipitation declines (Figs. 3, S5).

5 Discussion

The Arctic Basin is drained by several rivers that receive runoff contributions over great distances, from grasslands and forests in the south to tundra in the north. Surface runoff has typically been a substantial component of river discharge, with subsurface flows characterizing low flows in summer and early fall. These characteristic patterns and dynamics are shifting due to influences from warming, primarily hydrological cycle intensification and permafrost thaw. The shifts are altering the water cycle from processes manifesting both horizontally via primarily atmospheric effects, vertically from soil thaw, and seasonally through a combination of both impacts. Recent research suggests that a warming Arctic will experience changes in moisture sources that will influence freshwater exports from rivers. The two coupled climate models from which outputs were used in this study capture substantial precipitation increases in regions adjacent to the Arctic Ocean. This is a robust feature of climate models that is linked to the Arctic Ocean being more open later this century (Barnhart et al., 2016; McCrystall

et al., 2021). River basins near the western Arctic Ocean, particularly far northeast Eurasia, northwest Canada, and northern Alaska, will experience relatively large increases in river discharge, driven partly by higher snowfall rates and spring SWE amounts. These are cold areas that will warm significantly and, in turn, increasingly be fed by additional moisture, including from more frequent atmospheric rivers (Zhang et al., 2023). In contrast, southern parts of the pan-Arctic basin are projected to experience a decline in net precipitation and runoff contributions to rivers. In general, rivers in central Eurasia and southern Canada will receive less runoff, particularly during summer. Our results suggest that nearly 90 % of the increase in river discharge from permafrost regions will arise from an increase in net precipitation (Cubasch et al., 2001) rather than a “dewatering” of permafrost from thawing soil ice, which likely also played a smaller role over the twentieth century (McClelland et al., 2004). This connection to net precipitation is consistent with attribution studies for the river discharge trends observed during the recent past (McClelland et al., 2004, 2006; Zhang et al., 2013). Our results point to significant shifts in sources of freshwater entering Arctic rivers, with less runoff to river networks in the south and more in the north. The headwaters of the large Arctic rivers like the Lena, Ob, Yenisei, and Mackenzie originate well south of what is typically considered Arctic lands. The simulations suggest that by end of century, some 20 %–30 % more freshwater discharge will enter, accumulate in, and be exported from the northern half of the four large rivers.

In addition to geographic shifts involving atmospheric influences, ongoing soil thaw and permafrost losses will also influence runoff and materials being contributed to rivers. Our results support a growing body of evidence that deepening active layers and losses in permafrost extent will increase subsurface runoff contributions to rivers. Permafrost extent declines by 42 % and 63 % (PWBM-MPI and PWBM-IPSL, respectively) between early-century (2000–2019) and late-century (2080–2099) periods, which is indicative of recent and future permafrost degradation. Recent observations in northern Alaska suggest that increased precipitation and deepening ALT play increasingly important roles in sustaining low flows and enhancing subsurface hydrologic processes (Arp et al., 2020; Cooper et al., 2023). Projected changes in subsurface runoff are more spatially variable compared to total runoff, though a similar south–north gradient exists. Increased subsurface runoff can lead to decreases in summer stream temperatures in headwater catchments (Sjöberg et al., 2021). Pronounced seasonal shifts in runoff contributions will also occur. Increased runoff in late spring will likely be driven by higher snow storage and earlier melt that will shift peak spring freshet runoff earlier by approximately 11 d this century. Increased autumn discharge in the simulations is not attributable to higher SWE, forced instead by thawing permafrost that is lengthening the period when flow occurs and creating deeper active layers that store

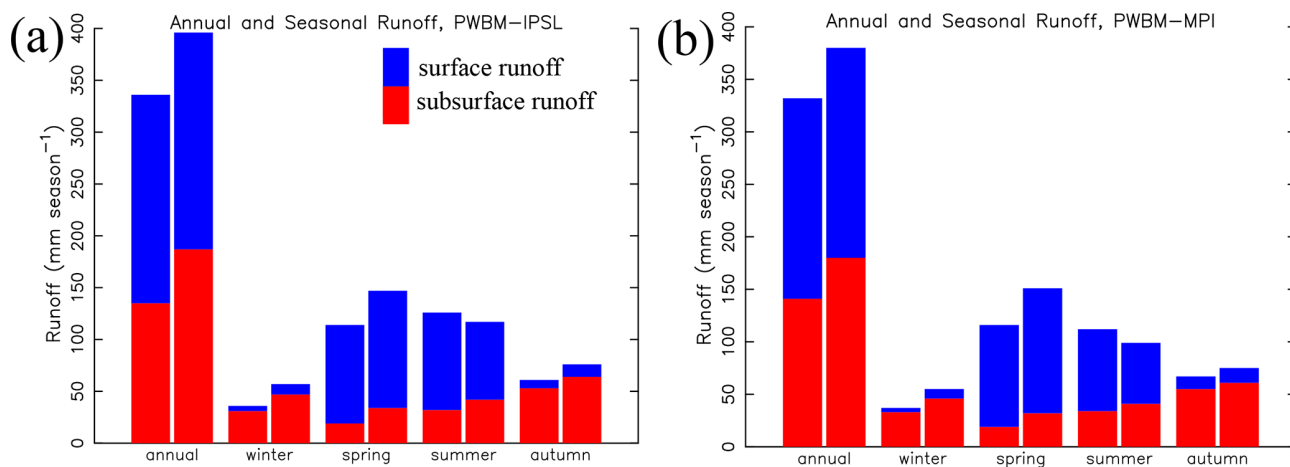


Figure 10. Annual and seasonal total runoff for the early-century (left bar for each period) and late-century (right bar for each period) periods, expressed as surface (blue) and subsurface (red) amounts for (a) PWBM-IPSL and (b) PWBM-MPI simulations.

and release water later in the season. More runoff during November and December, an approximate 5-fold increase in the modest warming simulation, highlights the physical connection between warming, permafrost degradation, and increasing subsurface flows to streams and rivers (St. Jacques and Sauchyn, 2009; Rawlins et al., 2019). The relatively large changes in November–April runoff described here are congruent with a recent study that documented a 10% per decade increase in cold-season discharge from nine rivers in Alaska with long data records (Blaskey et al., 2023). Warming, prominent in this region during autumn and early winter, can promote increased soil water storage, delaying the release of water into the streams and thus contributing to increases in winter flow (Streletskiy et al., 2015). Results of this study support the hypothesis that across the Arctic Basin subsurface runoff increases will be greatest in permafrost areas.

Taken together along with other studies (Mann et al., 2022; Tank et al., 2023), the spatial shifts suggest alterations in materials exported to coastal waters. Warming and higher rainfall rates will enhance thaw and increase coastal erosion. Higher runoff rates will drive additional subsurface contributions of freshwater and DOC to coastal seas and lagoons (Connolly et al., 2020). More cold-season river discharge has the potential to affect sea ice dynamics and other near-shore processes involving quantities such as salinity and biogeochemistry. The impacts extend to water quality and material exports by rivers. For example, DOC input to the Arctic Ocean has a very high temporal and geographical variability, with a strong bias towards the large Eurasian rivers and the freshet period (Amon et al., 2012). Our results suggest impacts to carbon of differing quality, as Amon et al. (2012) reported that the lignin phenol and *p*-hydroxybenzene composition of Arctic river DOC points to the abundance of young, boreal vegetation-derived leachates during spring flood and older, soil-, peat-, and wetland-derived DOC dur-

ing groundwater-dominated low-flow conditions. In northern tundra areas where soil carbon amounts are greater, warmer temperatures and increased runoff will likely lead to increased riverine DOC exports. Indeed, Frey and Smith (2005) concluded that, assuming no change in either river discharge or in-channel processes, warming would produce a 2.7–4.4 Tg yr⁻¹ increase in terrestrial DOC flux from western Siberia to the Arctic Ocean by 2100, with even larger increases likely should river discharge from the region continue to increase, as depicted in the simulations examined here. Warming and shifting snowmelt dynamics could increase transport and mobilization of DOC as subsurface pathways become active earlier in the year (Croghan et al., 2023). In contrast, some areas may experience a decrease in DOC export over time due to longer flow paths and residence times, along with increased microbial mineralization of DOC in the soil column (Striegl et al., 2005). Increasing soil thaw is expected to accelerate the release of old carbon (Dean et al., 2018; Schwab et al., 2020), which in turn will be entrained into, processed by, and exported from Arctic rivers. Moreover, DOC from deep sediments (> 3 m) could also become a significant contribution of carbon to Arctic rivers as the climate continues to warm (Mohammed et al., 2022). Nitrate concentrations are greater at lower latitudes as compared with higher latitudes where permafrost is more prominent (Frey and McClelland, 2009). Changes expressed predominantly across northern parts of the Arctic Basin will have a direct influence on coastal zone processes. On balance, our results point to continued increases in DOC export by Arctic rivers and to the mobilization and transport of ancient carbon in subsurface runoff from permafrost areas.

The use of two climate model forcing sets increases confidence in elements of the model outputs and the associated analysis. It is noteworthy that results involving runoff, in particular the spatial patterns, are similar between the two simulations. Magnitudes of air temperature and precipita-

tion increases are greater in the simulation forced with IPSL (PWBM-IPSL). Under those warmer temperatures, the Hamon potential evapotranspiration method captures the temperature dependence on actual and potential evapotranspiration. Higher precipitation rates in a warmer forcing scenario, like IPSL, are offset by higher simulated ET, resulting in relatively similar magnitudes of annual net precipitation and annual total runoff. This plausible modeling result suggests less uncertainty with the magnitudes of runoff changes compared with the changes in meteorological forcings projected by the climate models. The model validation analysis suggests that the magnitude of simulated annual total runoff and discharge is comparable to independent observational datasets, with time trends similar in magnitude to those reported in other studies.

Salient conclusions from this study come with caveats related to the limits of the analysis. Foremost is the large degree of uncertainty in meteorological data across Arctic regions, attributable to a sparse observation network and uncertainties in the magnitude of meteorological changes projected by the two coupled climate models. This uncertainty is ameliorated somewhat through the use of reanalysis data and model calibration. Results are implicitly linked to the connection between landscape runoff and river discharge export. Results are also influenced by the choice of climate model forced under the SSP3-7.0 scenario. In light of this, one might expect lower magnitudes of change should atmospheric greenhouse gas concentrations not rise to levels depicted in SSP3-7.0. The broad spatial extent and moderate model resolution (25×25 km grid cells) employed in this study limit our ability to incorporate influences such as thermokarst and talik formation on runoff contributions to streams and rivers. However, it is not clear that these local processes are a major component of riverine material exports by Arctic rivers (Dean et al., 2018). The model simulations do not include interactions between lakes and the river networks, so impacts from lake thaw drainage events (Smith et al., 2005; Andresen and Lougheed, 2015; Jones et al., 2022) are not simulated. The influence of land subsidence on soil temperature, moisture, and water storage is also not simulated. While subsidence is unlikely to lead to an abrupt thaw over large areas, it can have significant effects on the hydrology of polygonal tundra, generally increasing landscape runoff (Painter et al., 2023). The effect on large river basins will depend on the fraction of those basins that contain polygonal tundra. Our results underscore the importance in better understanding the myriad of transformations reshaping Arctic environments. Large changes in the far north emphasize the need for more frequent and spatially extensive sampling of small- and medium-sized rivers that ring the Arctic Ocean. Increased confidence in the magnitude of likely responses will require a multimodel, multi-scenario ensemble of simulations to obtain a range of projections consistent with known uncertainties. Incorporating small-scale effects such as thermokarst and lake drainage on river discharge will

require higher-resolution simulations. New model parameterization obtained from high-resolution remote-sensing observations will improve model capabilities in simulating permafrost hydrology in data-sparse regions of the Arctic.

Code and data availability. The W5E5 data are available at <https://doi.org/10.5880/pik.2019.023> (Lange, 2019b). The MERRA reanalysis data are available at <https://gmao.gsfc.nasa.gov/reanalysis/MERRA/> (last access: 23 January 2023, NASA, 2023). The ECMWF reanalysis v5 (ERA5) data are available at <https://www.ecmwf.int/en/forecasts/dataset/ecmwf-reanalysis-v5> (last access: 19 March 2023, ECMWF, 2023). The TPDC data are available at <https://data.tpdc.ac.cn/en/data/5093d9ff-a5fc-4f10-a53f-c01e7b781368/> (last access: 3 February 2023; Ran et al., 2022). The IPA permafrost data in the Circum-Arctic Map of Permafrost and Ground-Ice Conditions, Version 2 are available at <https://doi.org/10.7265/skbg-kf16> (Brown et al., 2002). The Global Land Evaporation Amsterdam Model (GLEAM) data are available at <https://www.gleam.eu/> (last access: 17 April 2023, GLEAM, 2023). The pan-Arctic ET data derived from remote sensing are available at http://files.ntsg.umt.edu/data/PA_Monthly_ET/ (last access: 16 April 2023; Numerical Terradynamic Simulation Group, 2023). Climate model data used as forcings are available in the ISIMIP repository located at <https://doi.org/10.48364/ISIMIP.342217> (Lange et al., 2021; Cucchi et al., 2020). Model source code, forcings, parameterizations, and outputs are available at <https://doi.org/10.15485/2290364> (Rawlins and Karmalkar, 2024).

Supplement. The supplement related to this article is available online at: <https://doi.org/10.5194/tc-18-1033-2024-supplement>.

Author contributions. MAR set up and executed the simulations, analyzed the results, and wrote the initial draft. AVK prepared the modeling forcing datasets and contributed to the analysis and writing of the accepted article.

Competing interests. The contact author has declared that neither of the authors has any competing interests.

Disclaimer. Publisher's note: Copernicus Publications remains neutral with regard to jurisdictional claims made in the text, published maps, institutional affiliations, or any other geographical representation in this paper. While Copernicus Publications makes every effort to include appropriate place names, the final responsibility lies with the authors.

Special issue statement. This article is part of the special issue "Northern hydrology in transition – impacts of a changing cryosphere on water resources, ecosystems, and humans (TC/HESS inter-journal SI)". It is not associated with a conference.

Acknowledgements. The PWBM simulations were performed on high-performance computing resources provided by the Massachusetts Green High Performance Computing Center. We thank John Kimball, James McClelland, Vladimir Alexeev, the two reviewers, and the editor for comments which greatly improved the paper.

Financial support. This research has been supported by the U.S. Department of Energy, Office of Science, Office of Biological and Environmental Research (grant no. DE-SC0019462), the National Aeronautics and Space Administration (grant no. 80NSSC19K0649), and the U.S. National Science Foundation, Division of Polar Programs (grant no. NSF-OPP-1656026).

Review statement. This paper was edited by Ylva Sjöberg and reviewed by two anonymous referees.

References

- Ahmed, R., Prowse, T., Dibike, Y., Bonsal, B., and O'Neil, H.: Recent Trends in Freshwater Influx to the Arctic Ocean from Four Major Arctic-Draining Rivers, *Water*, 12, 1189, <https://doi.org/10.3390/w12041189>, 2020.
- Alexeev, V., Nicolsky, D., Romanovsky, V., and Lawrence, D.: An evaluation of deep soil configurations in the CLM3 for improved representation of permafrost, *Geophys. Res. Lett.*, 34, L08501, <https://doi.org/10.1029/2007GL029536>, 2007.
- Amon, R. M. W., Rinehart, A. J., Duan, S., Louchouart, P., Prokushkin, A., Guggenberger, G., Bauch, D., Stedmon, C., Raymond, P. A., Holmes, R. M., McClelland, J. W., Peterson, B. J., Walker, S. J., and Zhulidov, A. V.: Dissolved organic matter sources in large Arctic rivers, *Geochim. Cosmochim. Ac.*, 94, 217–237, <https://doi.org/10.1016/j.gca.2012.07.015>, 2012.
- Andresen, C. G. and Lougheed, V. L.: Disappearing Arctic tundra ponds: Fine-scale analysis of surface hydrology in drained thaw lake basins over a 65 year period (1948–2013), *J. Geophys. Res.-Biogeo.*, 120, 466–479, <https://doi.org/10.1002/2014JG002778>, 2015.
- Anisimov, O. and Reneva, S.: Permafrost and Changing Climate: The Russian Perspective, *AMBIO*, 35, 169–175, [https://doi.org/10.1579/0044-7447\(2006\)35\[169:PACCTR\]2.0.CO;2](https://doi.org/10.1579/0044-7447(2006)35[169:PACCTR]2.0.CO;2), 2006.
- Arp, C., Whitman, M., Kemnitz, R., and Stuefer, S.: Evidence of hydrological intensification and regime change from northern Alaskan watershed runoff, *Geophys. Res. Lett.*, 47, e2020GL089186, <https://doi.org/10.1029/2020GL089186>, 2020.
- Arp, C. D. and Whitman, M. S.: Lake basins drive variation in catchment-scale runoff response over a decade of increasing rainfall in Arctic Alaska, *Hydrol. Process.*, 36, e14583, <https://doi.org/10.1002/hyp.14583>, 2022.
- Barnhart, K. R., Miller, C. R., Overeem, I., and Kay, J. E.: Mapping the future expansion of Arctic open water, *Nat. Clim. Change.*, 6, 280–285, <https://doi.org/10.1038/nclimate2848>, 2016.
- Behnke, M. I., McClelland, J. W., Tank, S. E., Kellerman, A. M., Holmes, R. M., Haghypour, N., Eglinton, T. I., Raymond, P. A., Suslova, A., Zhulidov, A. V., Gurtovaya, T., Zimov, N., Zimov, S., Mutter, E. A., Amos, E., and Spencer, R. G. M.: Pan-Arctic Riverine Dissolved Organic Matter: Synchronous Molecular Stability, Shifting Sources and Subsidies, *Global Biogeochem. Cy.*, 35, e2020GB006871, <https://doi.org/10.1029/2020GB006871>, 2021.
- Bintanja, R.: The impact of Arctic warming on increased rainfall, *Sci. Rep.*, 8, 1–6, <https://doi.org/10.1038/s41598-018-34450-3>, 2018.
- Bintanja, R. and Selten, F. M.: Future increases in Arctic precipitation linked to local evaporation and sea-ice retreat, *Nature*, 509, 479–482, <https://doi.org/10.1038/nature13259>, 2014.
- Bintanja, R., van der Wiel, K., Van der Linden, E., Reusen, J., Bogerd, L., Krikken, F., and Selten, F.: Strong future increases in Arctic precipitation variability linked to poleward moisture transport, *Sci. Adv.*, 6, eaax6869, <https://doi.org/10.1126/sciadv.aax6869>, 2020.
- Biskaborn, B. K., Smith, S. L., Noetzli, J., Matthes, H., Vieira, G., Streletskiy, D. A., Schoeneich, P., Romanovsky, V. E., Lewkowicz, A. G., Abramov, A., Allard, M., Boike, J., Cable, W. L., Christiansen, H. H., Delaloye, R., Diekmann, B., Drozdov, D., Etzelmüller, B., Grosse, G., Guglielmin, M., Ingeman-Nielsen, T., Isaksen, K., Ishikawa, M., Johannsson, M., Johannsson, H., Joo, A., Kaverin, D., Kholodov, A., Konstantinov, P., Kröger, T., Lambiel, C., Lanckman, J.-P., Luo, D., Malkova, G., Meiklejohn, I., Moskalenko, N., Oliva, M., Phillips, M., Ramos, M., Sannel, A. B. K., Sergeev, D., Seybold, C., Skryabin, P., Vasiliev, A., Wu, Q., Yoshikawa, K., Zheleznyak, M., and Lantuit, H.: Permafrost is warming at a global scale, *Nat. Commun.*, 10, 1–11, <https://doi.org/10.1038/s41467-018-08240-4>, 2019.
- Blaskey, D., Koch, J. C., Gooseff, M. N., Newman, A. J., Cheng, Y., O'Donnell, J. A., and Musselman, K. N.: Increasing Alaskan river discharge during the cold season is driven by recent warming, *Environ. Res. Lett.*, 18, 024042, <https://doi.org/10.1088/1748-9326/acb661>, 2023.
- Box, J. E., Colgan, W. T., Christensen, T. R., Schmidt, N. M., Lund, M., Parmentier, F.-J. W., Brown, R., Bhatt, U. S., Euskirchen, E. S., Romanovsky, V. E., Walsh, J. E., Overland, J. E., Wang, M., Corell, R. W., Meier, W. N., Wouters, B., Mernild, S., Mård, J., Pawlak, J., and Olsen, M. S.: Key indicators of Arctic climate change: 1971–2017, *Environ. Res. Lett.*, 14, 045010, <https://doi.org/10.1088/1748-9326/aafc1b>, 2019.
- Bring, A., Asokan, S. M., Jaramillo, F., Jarsjö, J., Levi, L., Pietroni, J., Prieto, C., Rogberg, P., and Destouni, G.: Implications of freshwater flux data from the CMIP5 multimodel output across a set of Northern Hemisphere drainage basins, *Earth's Future*, 3, 206–217, <https://doi.org/10.1002/2014EF000296>, 2015.
- Brodzik, M. J. and Knowles, K.: EASE-Grid: A Versatile Set of Equal-Area Projections and Grids, in: *Discrete Global Grids*, edited by: Goodchild, M., Santa Barbara, CA, National Center for Geographic Information and Analysis, USA, <https://nsidc.org/data/user-resources/help-center/guide-ease-grids> (last access: 17 April 2023), 2002.
- Brown Jr., J. O. J. F., Heginbottom, J. A., and Melnikov, E. S.: Circum-Arctic Map of Permafrost and Ground-Ice Conditions, Tech. rep., National Snow and Ice Data Center/World Data Center for Glaciology, digital Media, revised 2001, 2001.
- Brown, J., Ferrians, O., Heginbottom, J. A., and Melnikov, E.: Circum-Arctic Map of Permafrost and Ground-Ice Conditions,

- Version 2, Boulder, Colorado USA, National Snow and Ice Data Center [data set], <https://doi.org/10.7265/skbg-kf16>, 2002.
- Burke, E. J., Zhang, Y., and Krinner, G.: Evaluating permafrost physics in the Coupled Model Intercomparison Project 6 (CMIP6) models and their sensitivity to climate change, *The Cryosphere*, 14, 3155–3174, <https://doi.org/10.5194/tc-14-3155-2020>, 2020.
- Christensen, T. R., Johansson, T., Åkerman, H. J., Mastepepanov, M., Malmer, N., Friberg, T., Crill, P., and Svensson, B. H.: Thawing sub-arctic permafrost: Effects on vegetation and methane emissions, *Geophys. Res. Lett.*, 31, L04501, <https://doi.org/10.1029/2003GL018680>, 2004.
- Ciliverd, H. M., White, D. M., Tidwell, A. C., and Rawlins, M. A.: The Sensitivity of Northern Groundwater Recharge to Climate Change: A Case Study in Northwest Alaska, *J. Am. Water Resour. Assoc.*, 47, 1–13, <https://doi.org/10.1111/j.1752-1688.2011.00569.x>, 2011.
- Connolly, C. T., Cardenas, M. B., Burkart, G. A., Spencer, R. G., and McClelland, J. W.: Groundwater as a major source of dissolved organic matter to Arctic coastal waters, *Nat. Commun.*, 11, 1–8, <https://doi.org/10.1038/s41467-020-15250-8>, 2020.
- Cooper, M. G., Zhou, T., Bennett, K. E., Bolton, W., Coon, E., Fleming, S. W., Rowland, J. C., and Schwenk, J.: Detecting Permafrost Active Layer Thickness Change From Nonlinear Baseflow Recession, *Water Resour. Res.*, 59, e2022WR033154, <https://doi.org/10.1029/2022WR033154>, 2023.
- Croghan, D., Ala-Aho, P., Lohila, A., Welker, J., Vuorenmaa, J., Kløve, B., Mustonen, K.-R., Aurela, M., and Marttila, H.: Coupling of Water-Carbon Interactions During Snowmelt in an Arctic Finland Catchment, *Water Resour. Res.*, 59, e2022WR032892, <https://doi.org/10.1029/2022WR032892>, 2023.
- Cubasch, U., Meehl, G., Boer, G., Stouffer, R., Dix, M., Noda, A., Senior, C., Raper, S., and Yap, K.: Projections of future climate change, in: *Climate Change 2001: The Scientific Basis: Contribution of Working Group I to the Third Assessment Report of the Intergovernmental Panel*, edited by: Houghton, J. T., Ding, Y., Griggs, D. J., Noguer, M., Van der Linden, P. J., Dai, X., Maskell, K., and Johnson, C. A., pp. 526–582, 2001.
- Cucchi, M., Weedon, G. P., Amici, A., Bellouin, N., Lange, S., Müller Schmied, H., Hersbach, H., and Buontempo, C.: WFDE5: bias-adjusted ERA5 reanalysis data for impact studies, *Earth Syst. Sci. Data*, 12, 2097–2120, <https://doi.org/10.5194/essd-12-2097-2020>, 2020.
- Dankers, R. and Middelkoop, H.: River discharge and freshwater runoff to the Barents Sea under present and future climate conditions, *Clim. Change*, 87, 131–153, 2008.
- Dean, J., van der Velde, Y., Garnett, M. H., Dinsmore, K. J., Baxter, R., Lessels, J. S., Smith, P., Street, L. E., Subke, J.-A., Tetzlaff, D., and Washbourne, I.: Abundant pre-industrial carbon detected in Canadian Arctic headwaters: implications for the permafrost carbon feedback, *Environ. Res. Lett.*, 13, 034024, <https://doi.org/10.1088/1748-9326/aaa1fe>, 2018.
- Debolskiy, M. V., Alexeev, V. A., Hock, R., Lammers, R. B., Shiklomanov, A., Schulla, J., Nicolovsky, D., Romanovsky, V. E., and Prusevich, A.: Water balance response of permafrost-affected watersheds to changes in air temperatures, *Environ. Res. Lett.*, 16, 084054, <https://doi.org/10.1088/1748-9326/ac12f3>, 2021.
- Del Vecchio, J. D., Palucis, M. C., and Meyer, C. R.: Permafrost extent sets drainage density in the Arctic, *P. Natl. Acad. Sci. USA*, 121, e2307072120, <https://doi.org/10.1073/pnas.2307072120>, 2024.
- Déry, S. J., Hernández-Henríquez, M. A., Burford, J. E., and Wood, E. F.: Observational evidence of an intensifying hydrological cycle in northern Canada, *Geophys. Res. Lett.*, 36, L13402, <https://doi.org/10.1029/2009GL038852>, 2009.
- Du, J., Kimball, J. S., and Jones, L. A.: Passive microwave remote sensing of soil moisture based on dynamic vegetation scattering properties for AMSR-E, *IEEE T. Geosci. Remote*, 54, 597–608, <https://doi.org/10.1109/TGRS.2015.2462758>, 2016.
- ECMWF: ECMWF Reanalysis v5 (ERA5), ECMWF [data set], <https://www.ecmwf.int/en/forecasts/dataset/ecmwf-reanalysis-v5>, last access: 19 March 2023.
- Feng, D., Gleason, C. J., Lin, P., Yang, X., Pan, M., and Ishitsuka, Y.: Recent changes to Arctic river discharge, *Nat. Commun.*, 12, 6917, <https://doi.org/10.1038/s41467-021-27228-1>, 2021.
- Ford, V. L. and Frauenfeld, O. W.: Arctic precipitation recycling and hydrologic budget changes in response to sea ice loss, *Global Planet. Change*, 209, 103752, <https://doi.org/10.1016/j.gloplacha.2022.103752>, 2022.
- Frey, K. E. and McClelland, J. W.: Impacts of permafrost degradation on arctic river biogeochemistry, *Hydrol. Process.*, 23, 169–182, <https://doi.org/10.1002/hyp.7196>, 2009.
- Frey, K. E. and Smith, L. C.: Amplified carbon release from vast West Siberian peatlands by 2100, *Geophys. Res. Lett.*, 32, L09401, <https://doi.org/10.1029/2004GL022025>, 2005.
- GLEAM: Global Land Evaporation Amsterdam Model, GLEAM [data set], <https://www.gleam.eu/>, last access: 17 April 2023.
- Guo, D., Wang, A., Li, D., and Hua, W.: Simulation of Changes in the Near-Surface Soil Freeze/Thaw Cycle Using CLM4.5 With Four Atmospheric Forcing Data Sets, *J. Geophys. Res.-Atmos.*, 123, 2509–2523, <https://doi.org/10.1002/2017JD028097>, 2018.
- Hinzman, L. D., Deal, C. J., McGuire, A. D., Mernild, S. H., Polyakov, I. V., and Walsh, J. E.: Trajectory of the Arctic as an integrated system, *Ecol. Appl.*, 23, 1837–1868, <https://doi.org/10.1890/11-1498.1>, 2013.
- Hodson, T. O.: Root-mean-square error (RMSE) or mean absolute error (MAE): when to use them or not, *Geosci. Model Dev.*, 15, 5481–5487, <https://doi.org/10.5194/gmd-15-5481-2022>, 2022.
- Hu, Y., Ma, R., Sun, Z., Zheng, Y., Pan, Z., and Zhao, L.: Groundwater Plays an Important Role in Controlling Riverine Dissolved Organic Matter in a Cold Alpine Catchment, the Qinghai-Tibet Plateau, *Water Resour. Res.*, 59, e2022WR032426, <https://doi.org/10.1029/2022WR032426>, 2023.
- Hugelius, G., Tarnocai, C., Broll, G., Canadell, J. G., Kuhry, P., and Swanson, D. K.: The Northern Circumpolar Soil Carbon Database: spatially distributed datasets of soil coverage and soil carbon storage in the northern permafrost regions, *Earth Syst. Sci. Data*, 5, 3–13, <https://doi.org/10.5194/essd-5-3-2013>, 2013.
- Huntington, T. G.: Evidence for intensification of the global water cycle: Review and synthesis, *J. Hydrol.*, 319, 83–95, <https://doi.org/10.1016/j.jhydrol.2005.07.003>, 2006.
- Huntington, T. G.: Climate Warming-Induced Intensification of the Hydrologic Cycle: An Assessment of the Published Record and Potential Impacts on Agriculture, *Adv. Agron.*, 109, 1–53, <https://doi.org/10.1016/B978-0-12-385040-9.00001-3>, 2010.

- Jin, H., Huang, Y., Bense, V. F., Ma, Q., Marchenko, S. S., Shepelev, V. V., Hu, Y., Liang, S., Spektor, V. V., Jin, X., Li, X., and Li, X.: Permafrost Degradation and Its Hydrogeological Impacts, *Water*, 14, 372, <https://doi.org/10.3390/w14030372>, 2022.
- Jones, B. M., Grosse, G., Farquharson, L. M., Roy-Léveillé, P., Veremeeva, A., Kanevskiy, M. Z., Gaglioti, B. V., Breen, A. L., Parsekian, A. D., Ulrich, M., and Hinkel, K. M.: Lake and drained lake basin systems in lowland permafrost regions, *Nat. Rev. Earth Environ.*, 3, 85–98, <https://doi.org/10.1038/s43017-021-00238-9>, 2022.
- Koch, J. C., Bogard, M. J., Butman, D. E., Finlay, K., Ebel, B., James, J., Johnston, S. E., Jorgenson, M. T., Pastick, N. J., Spencer, R. G., Striegl, R., Walvoord, M., and Wickland, K. P.: Heterogeneous Patterns of Aged Organic Carbon Export Driven by Hydrologic Flow Paths, Soil Texture, Fire, and Thaw in Discontinuous Permafrost Headwaters, *Global Biogeochem. Cy.*, 36, e2021GB007242, <https://doi.org/10.1029/2021GB007242>, 2022.
- Koven, C. D., Riley, W. J., and Stern, A.: Analysis of Permafrost Thermal Dynamics and Response to Climate Change in the CMIP5 Earth System Models, *J. Climate*, 26, 1877–1900, <https://doi.org/10.1175/JCLI-D-12-00228.1>, 2013.
- Lafrenière, M. J. and Lamoureux, S. F.: Effects of changing permafrost conditions on hydrological processes and fluvial fluxes, *Earth-Sci. Rev.*, 191, 212–223, <https://doi.org/10.1016/j.earscirev.2019.02.018>, 2019.
- Lange, S.: Trend-preserving bias adjustment and statistical downscaling with ISIMIP3BASD (v1.0), *Geosci. Model Dev.*, 12, 3055–3070, <https://doi.org/10.5194/gmd-12-3055-2019>, 2019a.
- Lange, S.: WFDE5 over land merged with ERA5 over the ocean (W5E5). V. 1.0. GFZ Data Services [data set], <https://doi.org/10.5880/pik.2019.023>, 2019b.
- Lange, S.: ISIMIP3BASD, Zenodo [data set], <https://doi.org/10.5281/zenodo.4686991>, 2021.
- Lange, S., Menz, C., Gleixner, S., Cucchi, M., Weedon, G. P., Amici, A., Bellouin, N., Schmied, H. M., Hersbach, H., Buontempo, C., and Cagnazzo, C.: WFDE5 over land merged with ERA5 over the ocean (W5E5 v2.0), ISIMIP [data set], <https://doi.org/10.48364/ISIMIP.342217>, 2021.
- Lawrence, D. M. and Slater, A. G.: Incorporating organic soil into a global climate model, *Clim. Dynam.*, 30, 145–160, <https://doi.org/10.1007/s00382-007-0278-1>, 2008.
- Liljedahl, A. K., Boike, J., Daanen, R. P., Fedorov, A. N., Frost, G. V., Grosse, G., Hinzman, L. D., Iijima, Y., Jorgenson, J. C., Matveyeva, N., Necsoiu, M., Reynolds, M. K., Romanovsky, V. E., Schulla, J., Tape, K. D., Walker, D. A., Wilson, C. J., Yabuki H., and Zona, D.: Pan-Arctic ice-wedge degradation in warming permafrost and its influence on tundra hydrology, *Nat. Geosci.*, 9, 312–318, <https://doi.org/10.1038/ngeo2674>, 2016.
- Liston, G. E., Haehnel, R. B., Sturm, M., Hiemstra, C. A., Berezhovskaya, S., and Tabler, R. D.: Simulating complex snow distributions in windy environments using SnowTran-3D, *J. Glaciol.*, 53, 241–256, <https://doi.org/10.3189/172756507782202865>, 2007.
- Liu, S., Wang, P., Yu, J., Wang, T., Cai, H., Huang, Q., Pozdniakov, S. P., Zhang, Y., and Kazak, E. S.: Mechanisms behind the uneven increases in early, mid-and late winter streamflow across four Arctic river basins, *J. Hydrol.*, 606, 127425, <https://doi.org/10.1016/j.jhydrol.2021.127425>, 2022.
- Mann, P. J., Strauss, J., Palmtag, J., Dowdy, K., Ogneva, O., Fuchs, M., Bedington, M., Torres, R., Polimene, L., Overduin, P., Mollenhauer, G., Grosse, G., Rachold, V., Sobczak, W., Spencer, R., and Juhls, B.: Degrading permafrost river catchments and their impact on Arctic Ocean nearshore processes, *Ambio*, 51, 439–455, <https://doi.org/10.1007/s13280-021-01666-z>, 2022.
- Martens, B., Miralles, D. G., Lievens, H., van der Schalie, R., de Jeu, R. A. M., Fernández-Prieto, D., Beck, H. E., Dorigo, W. A., and Verhoest, N. E. C.: GLEAM v3: satellite-based land evaporation and root-zone soil moisture, *Geosci. Model Dev.*, 10, 1903–1925, <https://doi.org/10.5194/gmd-10-1903-2017>, 2017.
- McClelland, J. W., Holmes, R. M., Peterson, B. J., and Stieglitz, M.: Increasing river discharge in the Eurasian Arctic: Consideration of dams, permafrost thaw, and fires as potential agents of change, *J. Geophys. Res.-Atmos.*, 109, D18102, <https://doi.org/10.1029/2004JD004583>, 2004.
- McClelland, J. W., Déry, S. J., Peterson, B. J., Holmes, R. M., and Wood, E. F.: A pan-arctic evaluation of changes in river discharge during the latter half of the 20th century, *Geophys. Res. Lett.*, 33, L06715, <https://doi.org/10.1029/2006GL025753>, 2006.
- McCrystall, M. R., Stroeve, J., Serreze, M., Forbes, B. C., and Screen, J. A.: New climate models reveal faster and larger increases in Arctic precipitation than previously projected, *Nat. Commun.*, 12, 6765, <https://doi.org/10.1038/s41467-021-27031-y>, 2021.
- McKenzie, J. M., Kurylyk, B. L., Walvoord, M. A., Bense, V. F., Fortier, D., Spence, C., and Grenier, C.: Invited perspective: What lies beneath a changing Arctic?, *The Cryosphere*, 15, 479–484, <https://doi.org/10.5194/tc-15-479-2021>, 2021.
- Miralles, D. G., Holmes, T. R. H., De Jeu, R. A. M., Gash, J. H., Meesters, A. G. C. A., and Dolman, A. J.: Global land-surface evaporation estimated from satellite-based observations, *Hydrol. Earth Syst. Sci.*, 15, 453–469, <https://doi.org/10.5194/hess-15-453-2011>, 2011.
- Mohammed, A. A., Guimond, J. A., Bense, V. F., Jamieson, R. C., McKenzie, J. M., and Kurylyk, B. L.: Mobilization of subsurface carbon pools driven by permafrost thaw and reactivation of groundwater flow: a virtual experiment, *Environ. Res. Lett.*, 17, 124036, <https://doi.org/10.1088/1748-9326/aca701>, 2022.
- NASA: Modern-Era Retrospective analysis for Research and Applications (MERRA), NASA [data set], <https://gmao.gsfc.nasa.gov/reanalysis/MERRA/>, last access: 23 January 2023.
- Nash, D., Waliser, D., Guan, B., Ye, H., and Ralph, F. M.: The Role of Atmospheric Rivers in Extratropical and Polar Hydroclimate, *J. Geophys. Res.-Atmos.*, 123, 6804–6821, <https://doi.org/10.1029/2017JD028130>, 2018.
- Ni, J., Wu, T., Zhu, X., Hu, G., Zou, D., Wu, X., Li, R., Xie, C., Qiao, Y., Pang, Q., Hao, J., and Yang, C.: Simulation of the Present and Future Projection of Permafrost on the Qinghai-Tibet Plateau with Statistical and Machine Learning Models, *J. Geophys. Res.-Atmos.*, 126, e2020JD033402, <https://doi.org/10.1029/2020JD033402>, 2021.
- Nicolosky, D., Romanovsky, V., Alexeev, V., and Lawrence, D.: Improved modeling of permafrost dynamics in a GCM land-surface scheme, *Geophys. Res. Lett.*, 34, L08501, <https://doi.org/10.1029/2007GL029525>, 2007.
- Numerical Terradynamic Simulation Group: Pan-Arctic Evapotranspiration Data, Numerical Terradynamic Simulation Group,

- University of Montana [data set], http://files.ntsg.umt.edu/data/PA_Monthly_ET/, last access: 16 April 2023.
- Overland, J., Dunlea, E., Box, J. E., Corell, R., Forsius, M., Kattsov, V., Olsen, M. S., Pawlak, J., Reiersen, L.-O., and Wang, M.: The urgency of Arctic change, *Polar Sci.*, 21, 6–13, <https://doi.org/10.1016/j.polar.2018.11.008>, 2019.
- Painter, S. L., Coon, E. T., Khattak, A. J., and Jastrow, J. D.: Drying of tundra landscapes will limit subsidence-induced acceleration of permafrost thaw, *P. Natl. Acad. Sci. USA*, 120, e2212171120, <https://doi.org/10.1073/pnas.2212171120>, 2023.
- Peng, X., Zhang, T., Frauenfeld, O. W., Wang, K., Luo, D., Cao, B., Su, H., Jin, H., and Wu, Q.: Spatiotemporal Changes in Active Layer Thickness under Contemporary and Projected Climate in the Northern Hemisphere, *J. Climate*, 31, 251–266, <https://doi.org/10.1175/JCLI-D-16-0721.1>, 2018.
- Peterson, B. J., Holmes, R. M., McClelland, J. W., Vörösmarty, C. J., Lammers, R. B., Shiklomanov, A. I., Shiklomanov, I. A., and Rahmstorf, S.: Increasing River Discharge to the Arctic Ocean, *Science*, 298, 2171–2173, <https://doi.org/10.1126/science.1077445>, 2002.
- Ran, Y., Li, X., Cheng, G., Che, J., Aalto, J., Karjalainen, O., Hjort, J., Luoto, M., Jin, H., Obu, J., Hori, M., Yu, Q., and Chang, X.: New high-resolution estimates of the permafrost thermal state and hydrothermal conditions over the Northern Hemisphere, *Earth Syst. Sci. Data*, 14, 865–884, <https://doi.org/10.5194/essd-14-865-2022>, 2022 (data available at: <https://data.tpdc.ac.cn/en/data/5093d9ff-a5fc-4f10-a53f-c01e7b781368/>, last access: 3 February 2023).
- Rantanen, M., Karpechko, A. Y., Lipponen, A., Nordling, K., Hyvärinen, O., Ruosteenoja, K., Vihma, T., and Laaksonen, A.: The Arctic has warmed nearly four times faster than the globe since 1979, *Commun. Earth Environ.*, 3, 168, <https://doi.org/10.1038/s43247-022-00498-3>, 2022.
- Rawlins, M. and Karmalkar, A.: Modeled estimates of permafrost hydrology and related fields for pan-Arctic region over the period 1980–2100. Quantifying Variability and Controls of Riverine Dissolved Organic Carbon Exported to Arctic Coastal Margins of North America, ESS-DIVE repository [code and data set], <https://doi.org/10.15485/2290364>, 2024.
- Rawlins, M. A.: Increasing freshwater and dissolved organic carbon flows to Northwest Alaska's Elson lagoon, *Environ. Res. Lett.*, 16, 105014, <https://doi.org/10.1088/1748-9326/ac2288>, 2021.
- Rawlins, M. A., Lammers, R. B., Frothing, S., Fekete, B. M., and Vörösmarty, C. J.: Simulating Pan-Arctic Runoff with a Macro-Scale Terrestrial Water Balance Model, *Hydrol. Process.*, 17, 2521–2539, <https://doi.org/10.1002/hyp.1271>, 2003.
- Rawlins, M. A., Steele, M., Holland, M. M., Adam, J. C., Cherry, J. E., Francis, J. A., Groisman, P. Y., Hinzman, L. D., Huntington, T. G., Kane, D. L., Kamball, J. S., Kwok, R., Lammers, R. B., Lee, C. M., Lettenmaier, D. P., McDonald, K. C., Podest, E., Pundsack, J. W., Rudels, B., Serreze, M. C., Shiklomanov, A., Skagseth, Ø., Troy, T. J., Vörösmarty, C. J., Wensnahan, M., Wood, E. F., Woodgate, R., Yang, D., Zhang, K., and Zhang, T.: Analysis of the Arctic System for Freshwater Cycle Intensification: Observations and Expectations, *J. Climate*, 23, 5715–5737, <https://doi.org/10.1175/2010JCLI3421.1>, 2010.
- Rawlins, M. A., Nicolsky, D. J., McDonald, K. C., and Romanovsky, V. E.: Simulating soil freeze/thaw dynamics with an improved pan-Arctic water balance model, *J. Adv. Model. Earth Sy.*, 5, 659–675, <https://doi.org/10.1002/jame.20045>, 2013.
- Rawlins, M. A., Cai, L., Stuefer, S. L., and Nicolsky, D.: Changing characteristics of runoff and freshwater export from watersheds draining northern Alaska, *The Cryosphere*, 13, 3337–3352, <https://doi.org/10.5194/tc-13-3337-2019>, 2019.
- Rawlins, M. A., Connolly, C. T., and McClelland, J. W.: Modeling Terrestrial Dissolved Organic Carbon Loading to Western Arctic Rivers, *J. Geophys. Res.-Biogeo.*, 126, e2021JG006420, <https://doi.org/10.1029/2021JG006420>, 2021.
- Sazonova, T. S. and Romanovsky, V. E.: A model for regional-scale estimation of temporal and spatial variability of active layer thickness and mean annual ground temperatures, *Permafrost Periglac.*, 14, 125–139, <https://doi.org/10.1002/ppp.449>, 2003.
- Schroeder, R., McDonald, K. C., Zimmerman, R., Podest, E., and Rawlins, M.: North Eurasian Inundation Mapping with Passive and Active Microwave Remote Sensing, *Environ. Res. Lett.*, 5, 015003, <https://doi.org/10.1088/1748-9326/5/1/015003>, 2010.
- Schwab, M. S., Hilton, R. G., Raymond, P. A., Haghipour, N., Amos, E., Tank, S. E., Holmes, R. M., Tipper, E. T., and Eglinton, T. I.: An Abrupt Aging of Dissolved Organic Carbon in Large Arctic Rivers, *Geophys. Res. Lett.*, 47, e2020GL088823, <https://doi.org/10.1029/2020GL088823>, 2020.
- Serreze, M. C. and Meier, W. N.: The Arctic's sea ice cover: trends, variability, predictability, and comparisons to the Antarctic, *Ann. N. Y. Acad. Sci.*, 1436, 36–53, <https://doi.org/10.1111/nyas.13856>, 2019.
- Shapiro, S. S. and Wilk, M. B.: An analysis of variance test for normality (complete samples), *Biometrika*, 52, 591–611, <https://doi.org/10.2307/2333709>, 1965.
- Shiklomanov, A. I., Lammers, R. B., Lettenmaier, D. P., Polischuk, Y. M., Savichev, O. G., Smith, L. C., and Chernokulsky, A. V.: Hydrological Changes: Historical Analysis, Contemporary Status, and Future Projections, *Regional Environmental Changes in Siberia and Their Global Consequences*, Springer, 111–154, https://doi.org/10.1007/978-94-007-4569-8_4, 2013.
- Shiklomanov, I. A. and Shiklomanov, A. I.: Climatic Change and Dynamics of River Discharge into the Arctic Ocean, *Water Resour.*, 30, 593–601, 2003.
- Shiklomanov, I. A., Shiklomanov, A. I., Lammers, R. B., Peterson, B. J., and Vörösmarty, C. J.: The dynamics of river water inflow to the Arctic Ocean, in: *The Freshwater Budget of the Arctic Ocean*, edited by: Lewis, E. L., Jones, E. P., Lemke, P., Prowse, T. D., and Wadhams, P., 281–296, Kluwer Academic Press, Dordrecht, 2000.
- Sjöberg, Y., Jan, A., Painter, S. L., Coon, E. T., Carey, M. P., O'Donnell, J. A., and Koch, J. C.: Permafrost Promotes Shallow Groundwater Flow and Warmer Headwater Streams, *Water Resour. Res.*, 57, e2020WR027463, <https://doi.org/10.1029/2020WR027463>, 2021.
- Slater, A. G. and Lawrence, D. M.: Diagnosing Present and Future Permafrost from Climate Models, *J. Climate*, 26, 5608–5623, <https://doi.org/10.1175/JCLI-D-12-00341.1>, 2013.
- Smith, L. C., Sheng, Y., MacDonald, G. M., and Hinzman, L. D.: Disappearing Arctic Lakes, *Science*, 308, 1429, <https://doi.org/10.1029/2004JD005518>, 2005.
- Spencer, R. G., Mann, P. J., Dittmar, T., Eglinton, T. I., McIntyre, C., Holmes, R. M., Zimov, N., and Stubbins, A.: Detecting the sig-

- nature of permafrost thaw in Arctic rivers, *Geophys. Res. Lett.*, 42, 2830–2835, <https://doi.org/10.1002/2015GL063498>, 2015.
- St. Jacques, J. M. and Sauchyn, D. J.: Increasing winter baseflow and mean annual streamflow from possible permafrost thawing in the Northwest Territories, Canada, *Geophys. Res. Lett.*, 36, L01401, <https://doi.org/10.1029/2008GL035822>, 2009.
- Streletskiy, D. A., Tananaev, N. I., Opel, T., Shiklomanov, N. I., Nyland, K. E., Streletskaya, I. D., Tokarev, I., and Shiklomanov, A. I.: Permafrost hydrology in changing climatic conditions: seasonal variability of stable isotope composition in rivers in discontinuous permafrost, *Environ. Res. Lett.*, 10, 095003, <https://doi.org/10.1088/1748-9326/10/9/095003>, 2015.
- Striegl, R. G., Aiken, G. R., Dornblaser, M. M., Raymond, P. A., and Wickland, K. P.: A decrease in discharge-normalized DOC export by the Yukon River during summer through autumn, *Geophys. Res. Lett.*, 32, L21413, <https://doi.org/10.1029/2005GL024413>, 2005.
- Stroeve, J. and Notz, D.: Changing state of Arctic sea ice across all seasons, *Environ. Res. Lett.*, 13, 103001, <https://doi.org/10.1088/1748-9326/aade56>, 2018.
- Sturm, M. J., Holmgren, J., and Liston, G. E.: A Seasonal Snow Cover Classification System for Local to Global Applications, *J. Climate*, 8, 1261–1283, [https://doi.org/10.1175/1520-0442\(1995\)008<1261:ASSCCS>2.0.CO;2](https://doi.org/10.1175/1520-0442(1995)008<1261:ASSCCS>2.0.CO;2), 1995.
- Tananaev, N., Makarieva, O., and Lebedeva, L.: Trends in annual and extreme flows in the Lena River basin, Northern Eurasia, *Geophys. Res. Lett.*, 43, 10764–10772, <https://doi.org/10.1002/2016GL070796>, 2016.
- Tananaev, N., Teisserenc, R., and Debolskiy, M.: Permafrost Hydrology Research Domain: Process-Based Adjustment, *Hydrology*, 7, 6, <https://doi.org/10.3390/hydrology7010006>, 2020.
- Tank, S. E., Striegl, R. G., McClelland, J. W., and Kokelj, S. V.: Multi-decadal increases in dissolved organic carbon and alkalinity flux from the Mackenzie drainage basin to the Arctic Ocean, *Environ. Res. Lett.*, 11, 054015, <https://doi.org/10.1088/1748-9326/11/5/054015>, 2016.
- Tank, S. E., McClelland, J. W., Spencer, R. G., Shiklomanov, A. I., Suslova, A., Moatar, F., Amon, R. M., Cooper, L. W., Elias, G., Gordeev, V. V., Guay, C., Gurtovaya, T. Y., Kosmenko, L. S., Mutter, E. A., Peterson, B. J., Peucker-Ehrenbrink, B., Raymond, P. A., Schuster, P. F., Scott, L., Staples, R., Striegl, R. G., Tretiakov, M., Zhulidov, A. V., Zimov, N., Zimov, S., and Holmes, R. M.: Recent trends in the chemistry of major northern rivers signal widespread Arctic change, *Nat. Geosci.*, 16, 1–8, <https://doi.org/10.1038/s41561-023-01247-7>, 2023.
- Wagner, A., Lohmann, G., and Prange, M.: Arctic river discharge trends since 7 ka BP, *Global Planet. Change*, 79, 48–60, <https://doi.org/10.1016/j.gloplacha.2011.07.006>, 2011.
- Walsh, J. E., Chapman, W. L., Romanovsky, V., Christensen, J. H., and Stendel, M.: Global climate model performance over Alaska and Greenland, *J. Climate*, 21, 6156–6174, <https://doi.org/10.1175/2008JCLI2163.1>, 2008.
- Walvoord, M. A. and Kurylyk, B. L.: Hydrologic impacts of thawing permafrost—A review, *Vadose Zone J.*, 15, vjz2016.01.0010, <https://doi.org/10.2136/vjz2016.01.0010>, 2016.
- Walvoord, M. A. and Striegl, R. G.: Increased groundwater to stream discharge from permafrost thawing in the Yukon River basin: Potential impacts on lateral export of carbon and nitrogen, *Geophys. Res. Lett.*, 34, L12402, <https://doi.org/10.1029/2007GL030216>, 2007.
- Wang, P., Huang, Q., Pozdniakov, S. P., Liu, S., Ma, N., Wang, T., Zhang, Y., Yu, J., Xie, J., Fu, G., Frolova, N. L., and Liu, C.: Potential role of permafrost thaw on increasing Siberian river discharge, *Environ. Res. Lett.*, 16, 034046, <https://doi.org/10.1088/1748-9326/abe326>, 2021.
- Wang, Y.-R., Hessen, D. O., Samset, B. H., and Stordal, F.: Evaluating global and regional land warming trends in the past decades with both MODIS and ERA5-Land land surface temperature data, *Remote Sens. Environ.*, 280, 113181, <https://doi.org/10.1016/j.rse.2022.113181>, 2022.
- Warszawski, L., Frieler, K., Huber, V., Piontek, F., Serdeczny, O., and Schewe, J.: The inter-sectoral impact model intercomparison project (ISI-MIP): project framework, *P. Natl. Acad. Sci. USA*, 111, 3228–3232, <https://doi.org/10.1073/pnas.1312330110>, 2014.
- Willmott, C. J. and Matsuura, K.: Advantages of the mean absolute error (MAE) over the root mean square error (RMSE) in assessing average model performance, *Clim. Res.*, 30, 79–82, 2005.
- Willmott, C. J. and Matsuura, K.: Terrestrial Precipitation: 1900–2008 Gridded Monthly Time Series, Version 2.01, https://psl.noaa.gov/data/gridded/data/UDel_AirT_Precip.html (last access: 3 February 2023), 2009.
- Woo, M.-K., Kane, D. L., Carey, S. K., and Yang, D.: Progress in permafrost hydrology in the new millennium, *Permafrost Periglac.*, 19, 237–254, <https://doi.org/10.1002/ppp.613>, 2008.
- Yi, Y., Chen, R. H., Kimball, J. S., Moghaddam, M., Xu, X., Euskirchen, E. S., Das, N., and Miller, C. E.: Potential Satellite Monitoring of Surface Organic Soil Properties in Arctic Tundra From SMAP, *Water Resour. Res.*, 58, e2021WR030957, <https://doi.org/10.1029/2021WR030957>, 2022.
- Zhang, K., Kimball, J. S., Mu, Q., Jones, L. A., Goetz, S. J., and Running, S. W.: Satellite based analysis of northern ET trends and associated changes in the regional water balance from 1983 to 2005, *J. Hydrol.*, 379, 92–110, <https://doi.org/10.1016/j.jhydrol.2009.09.047>, 2009.
- Zhang, P., Chen, G., Ting, M., Ruby Leung, L., Guan, B., and Li, L.: More frequent atmospheric rivers slow the seasonal recovery of Arctic sea ice, *Nat. Clim. Change.*, 13, 266–273, <https://doi.org/10.1038/s41558-023-01599-3>, 2023.
- Zhang, S.-M., Mu, C.-C., Li, Z.-L., Dong, W.-W., Wang, X.-Y., Streletskaya, I., Grebenets, V., Sokratov, S., Kizyakov, A., and Wu, X.-D.: Export of nutrients and suspended solids from major Arctic rivers and their response to permafrost degradation, *Adv. Clim. Chang.*, 12, 466–474, <https://doi.org/10.1016/j.accre.2021.06.002>, 2021.
- Zhang, X., He, J., Zhang, J., Polyakov, I., Gerdes, R., Inoue, J., and Wu, P.: Enhanced poleward moisture transport and amplified northern high-latitude wetting trend, *Nat. Clim. Change.*, 3, 47–51, <https://doi.org/10.1038/nclimate1631>, 2013.